

NACA RM L54L28

~~CONFIDENTIAL~~  
**NACA**

# RESEARCH MEMORANDUM

TRANSONIC WIND-TUNNEL INVESTIGATION OF THE EFFECTS OF  
TAPER RATIO AND BODY INDENTATION ON THE AERODYNAMIC  
LOADING CHARACTERISTICS OF A 45° SWEEPBACK WING  
IN THE PRESENCE OF A BODY

By James B. Delano and John P. Mugler, Jr.

Langley Aeronautical Laboratory  
Langley Field, Va.

~~CONFIDENTIAL~~  
**UNCLASSIFIED**

To \_\_\_\_\_

By authority of NACA Reabs officials  
FRN-121 Date Oct. 14, 1957

AMT 11-15-57

CLASSIFIED DOCUMENT

This material contains information affecting the National Defense of the United States within the meaning of the espionage laws, TITLE 18, U.S.C., Secs. 793 and 794, the transmission or revelation of which in any manner to an unauthorized person is prohibited by law.

## NATIONAL ADVISORY COMMITTEE FOR AERONAUTICS

WASHINGTON

April 4, 1955

~~CONFIDENTIAL~~

## NATIONAL ADVISORY COMMITTEE FOR AERONAUTICS

## RESEARCH MEMORANDUM

TRANSONIC WIND-TUNNEL INVESTIGATION OF THE EFFECTS OF  
TAPER RATIO AND BODY INDENTATION ON THE AERODYNAMIC  
LOADING CHARACTERISTICS OF A 45° SWEEPBACK WING  
IN THE PRESENCE OF A BODY

By James B. Delano and John P. Mugler, Jr.

## SUMMARY

An investigation to determine the effects of taper ratio and body indentation on the aerodynamic loading characteristics of a 45° swept-back wing in the presence of a body was conducted in the Langley 8-foot transonic pressure tunnel at Mach numbers from 0.60 to 1.20 for angles of attack up to 20°. The wings employed had 45° sweepback of the 0.25-chord line, an aspect ratio of 4, NACA 65A006 airfoil sections, and taper ratios of 0.3 and 0.6, respectively.

An increase in taper ratio from 0.3 to 0.6 causes a delay in the Mach number for the transonic rearward and outboard movement of the center of pressure which results in maximum differences in the longitudinal and lateral locations of the order of 4 percent of the average chord and 3 percent of the wing semispan, respectively, around a Mach number of 1.0. In addition, a taper-ratio increase causes a delay in the wing normal-force coefficient at which pitch-up begins. Body indentation delayed slightly the Mach number for the start of the transonic rearward movement of the center of pressure. Good correlation of the effects of taper ratio on the longitudinal location of the center of pressure were obtained by utilizing the average chord as a reference in lieu of the mean aerodynamic chord. The division of load between the wing and the body was determined and is presented.

## INTRODUCTION

Designers of transonic and supersonic airplanes require knowledge of the effects of plan-form variables on the aerodynamic loading characteristics of wings at transonic speeds. Present theoretical methods for predicting the aerodynamic loadings for wings in this speed range

are not proven. Therefore, an experimental investigation of an exploratory nature was planned for the Langley 8-foot transonic pressure tunnel in which a strain-gage balance would be used to measure the wing normal force, bending moment, and pitching moment for several wing-body combinations. From these results, the location of the center of pressure of the wing was found as a function of Mach number and normal force; and for certain configurations, for which overall force test data are available, the division of normal-force and pitching-moment load between the wing and body was determined.

This investigation includes wings of different sweep, thickness, taper ratio, and incidence in order to determine the effects of the variation of these parameters on the aerodynamic loading characteristics at transonic speeds. Since appreciable aerodynamic gains are being obtained through the application of the transonic area rule (refs. 1 and 2), a study of the effect of body indentation on the loading characteristics is also included.

This paper presents the results of the first phase of this general investigation and shows the effects of taper ratio and body indentation on the wing loads for two swept wings having taper ratios of 0.3 and 0.6 but which are similar in all other respects.

#### SYMBOLS

A	aspect ratio
M	free-stream Mach number
$N_W$	normal force on the wing in the presence of the body, lb
$N_{WB}$	normal force on wing-body combination, lb
$M_W$	pitching moment of the wing in the presence of the body about 0.25 $\bar{c}$ , in-lb
$M_B$	bending moment for a wing panel in the presence of the body about body center line, in-lb
$C_{N_W}$	normal-force coefficient for the wing in the presence of the body, $N_W/qS$
$C_{N_{WB}}$	normal-force coefficient for wing-body combination, $N_{WB}/qS$
$C_{m_W}$	pitching-moment coefficient for the wing in the presence of the body, $M_W/qS\bar{c}$

- $C_B$  bending-moment coefficient for a wing panel in the presence of the body,  $M_B/q \frac{S}{2} \frac{b}{2}$
- $\frac{y}{b/2}$  lateral position of center of pressure in fraction of wing semispan measured from body center line,  $C_B/C_{N_W}$
- $(x/c)_{\bar{c}}$  longitudinal position of center of pressure in fraction of mean aerodynamic chord measured from leading edge of mean aerodynamic chord,  $0.25 - \frac{C_{m_W}}{C_{N_W}}$
- $(x/c)_{c_{av}}$  longitudinal position of center of pressure in fraction of average chord measured from leading edge of average chord,  $\frac{a}{c_{av}} - \frac{\bar{c}}{c_{av}} \frac{C_{m_W}}{C_{N_W}}$
- $\bar{c}$  wing mean aerodynamic chord,  $\frac{2}{S} \int_0^{b/2} c^2 dy$ , in.
- $\bar{c}_e$  wing mean aerodynamic chord for the exposed wing,  $\frac{2}{S_e} \int_{b/2-(b/2)_e}^{b/2} c^2 dy$ , in.
- $c$  wing local chord, in.
- $c_{av}$  wing average chord,  $\frac{c_t + c_r}{2}$ , in.
- $c_t$  wing-tip chord, in.
- $c_r$  wing-root chord at body center line, in.
- $b/2$  semispan of total wing, in.
- $(b/2)_e$  semispan of exposed wing, distance from wing tip to most inboard intersection of wing and body, in.
- $S$  area of total wing (including area blanketed by body), sq ft
- $S_e$  area of exposed wing, sq ft

- a longitudinal distance from leading edge of  $c_{av}$  to  $\bar{c}/4$   
(positive when moving downstream), in.
- x longitudinal distance parallel to model center line, in.
- y lateral distance measured perpendicular to model center  
line, in.
- $\alpha$  angle of attack of body center line, deg
- $\lambda$  taper ratio,  $c_t/c_r$
- $\rho$  free-stream mass density, slugs/cu ft
- q free-stream dynamic pressure,  $\rho V^2/2$ , lb/sq ft
- V free-stream velocity, ft/sec
- R Reynolds number based on wing average chord

## APPARATUS AND METHODS

### Tunnel

The present investigation was conducted in the Langley 8-foot transonic pressure tunnel. The test section of this tunnel is rectangular in cross section and has a cross-sectional area of approximately 50 square feet. The upper and lower walls of the test section are slotted to permit continuous operation through the transonic speed range. Some details of the test section are shown in figure 1. During this investigation, the tunnel was operated at approximately atmospheric stagnation pressure. The dewpoint of the tunnel air was controlled and was kept at approximately 0° F. The stagnation temperature of the tunnel air was automatically controlled and was kept constant and uniform across the tunnel at 120° F. Control of both dewpoint and stagnation temperature in this manner minimized humidity effects. The axial distribution of Mach number in the vicinity of the model was satisfactorily uniform at all test Mach numbers. Local deviations from the average stream Mach number were no larger than 0.005 at subsonic speeds. With increases in Mach number above 1.0, these deviations increased but did not exceed 0.010 in the region of the wing at the highest test Mach number of 1.20. Tests reported in reference 3 indicate that local flow nonuniformities of this magnitude have no effect on the measured force data. Some representative Mach number distributions at the center of the test section are presented in figure 2.

### Models

The 0.3-taper-ratio wing tested has  $45^\circ$  sweepback of the 0.25-chord line, an aspect ratio of 4, and NACA 65A006 airfoil sections parallel to the model plane of symmetry. The 0.6-taper-ratio wing has the same geometric characteristics as the aforementioned wing with the exception of the taper ratio. Both wings were of solid-steel construction, and both were tested as midwing configurations.

The body frame was constructed of steel and housed an internal strain-gage wing balance. The balance supported both left and right wings independent of the body. The balance measured bending moment on each wing and normal force and pitching moment for both wings. A photograph of the balance in the body is presented in figure 3. The outer shell of the body was constructed of plastic and fiber-glass-coated wood between body stations of 22.5 inches and 36.9 inches. The different body configurations were obtained by interchanging these outer plastic shells to form the desired contour. The shapes of the indented body configurations were obtained by application of the transonic area rule of references 1 and 2 for a Mach number of 1.0. The axial cross-sectional-area developments for the test configurations covered by this paper are presented as a portion of figure 2 of reference 4, since the shape of the bodies used for both tests was identical. Photographs and dimensional details of the wing-body combinations are presented in figures 4 and 5, respectively. Ordinates for the body configurations are presented in table I.

When the body shells were put into place, a gap of approximately 0.030 inch was left between the wing and the body shell in order that there would be no physical interference. To prevent any flow from entering the body through this gap, a rubber seal was provided at the wing-body juncture. (See fig. 5.) The effect of this seal on the balance-calibration constants was eliminated by balance calibrations with the seals in place. When the indented body configurations were tested, the thinner body shells did not allow enough thickness to provide an adequate seal. Therefore, the basic body configurations were tested with and without seals to evaluate the effect of the seals. The base of the bodies for both the basic and indented body configurations was closed to prevent any flow of air out of the base of the body.

An electrical system to determine if the body fouled the wing at high angles of attack was provided by painting the wing cutout in the body shell with a conductive silver paint. When the body fouled the wing, the circuit was made to an indicator light on the tunnel control panel. Data were not recorded under fouling conditions.

The model was connected to the tunnel central support system by means of a tapered sting attached at the base of the body (figs. 1 and 4(a)).

This support system was designed to keep the model near the center line of the tunnel throughout the angle-of-attack range.

#### Measurements and Accuracy

A study of the factors affecting the accuracy of the results indicates that the measured coefficients are accurate within the following limits:

M	$C_{N_W}$	$C_{m_W}$	$C_B$
0.6	0.009	0.004	0.008
1.2	.004	.002	.004

The average stream Mach number was held to within  $\pm 0.003$  of the nominal values shown on the figures; generally, this deviation did not exceed  $\pm 0.002$ . As previously mentioned in the tunnel-description section, the local deviations from the average stream Mach number ranged from 0.005 at subsonic speed to 0.010 at a Mach number of 1.20.

The angle of attack of the model was measured by a strain-gage attitude transmitter mounted in the model nose. Consideration of all of the factors affecting the accuracy indicates that the model angle of attack is accurate to within  $\pm 0.1^\circ$  relative to the free stream.

Measurements of the wing-tip angle of twist during the tests showed that the wing tips for both the 0.3- and 0.6-taper-ratio wings were operating at angles of attack less than the body center line of the order of  $1^\circ$  at the maximum loading conditions. Tests reported in reference 5 indicate that wing-tip twist angles of this order of magnitude have no effect on the measured force and moment coefficients.

Since the models tested were symmetrical, the moment-coefficient curves would be expected to pass through zero-moment coefficient at zero wing normal-force coefficient. Therefore, the moment-coefficient curves were shifted so as to pass through zero wing normal-force coefficient in the computing of the longitudinal and lateral center-of-pressure positions. This shift increased the accuracy of the computed center-of-pressure locations in the low range of the wing normal-force coefficient.

#### Wing-Balance Calibration

The wing balance was calibrated completely installed in the model in the tunnel test section as it would be used during the test. A

separate calibration was made for each model configuration. Examination of the calibration data revealed that the addition of seals to the basic wing-body configurations decreased the balance sensitivity by the order of 5 percent.

#### Configurations and Test Conditions

Four configurations were tested during this investigation. The specific configurations and test conditions are as follows:

- (1) 0.3-taper-ratio wing in the presence of the basic (unindented) body. Angle-of-attack range,  $0^{\circ}$  to  $20^{\circ}$ ; Mach number range, 0.60 to 1.12.
- (2) 0.6-taper-ratio wing in the presence of the basic (unindented) body. Angle-of-attack range,  $-2^{\circ}$  to  $20^{\circ}$ ; Mach number range, 0.60 to 1.20.
- (3) 0.3-taper-ratio wing in the presence of the indented body. Angle-of-attack range,  $0^{\circ}$  to  $20^{\circ}$ ; Mach number range, 0.60 to 1.20.
- (4) 0.6-taper-ratio wing in the presence of the indented body. Angle-of-attack range,  $0^{\circ}$  to  $20^{\circ}$ ; Mach number range, 0.60 to 1.20.

The Reynolds number based on the average wing chord was of the order of  $2 \times 10^6$  (fig. 6).

Test points were recorded with increases in angle of attack through  $20^{\circ}$  in every case where buffeting or balance load restrictions did not limit the testing range. In several instances where a slightly different model-support configuration was utilized to obtain the high-angle-of-attack data, repeat angles with both configurations were recorded to establish the correlation between the data obtained from both support configurations.

#### RESULTS

Force and moment coefficients for the 0.3- and 0.6-taper-ratio wings in the presence of the basic and indented bodies are presented for the Mach number range in figures 7 to 10. From these faired curves of force and moment coefficients, the longitudinal and lateral center-of-pressure locations have been determined and they are presented in figures 11 to 14. The division of load between the wing and the body was determined by analysis of the data presented herein in conjunction with data from reference 4 and unpublished data and is presented in figures 15 and 16. It was anticipated that utilization of the data from reference 4 along with force data for the body alone would allow the

body interference to be isolated. However, the electrical strain-gage balances utilized in these investigations were not sufficiently accurate to allow the relatively small interference effects to be separated from the overall effects.

In order to facilitate presentation of the data, staggered scales have been used in many figures, and care should be taken in selecting the zero axis for each curve.

## DISCUSSION

### Effect of Wing-Body-Juncture Seals

The force and moment coefficients for the wings in the presence of the basic body with and without the wing-body-juncture seal (figs. 7 and 8) generally show good agreement with the exception of the pitching-moment coefficients above pitch-up.

### General Effects

The following general effects are applicable to each of the four configurations tested; the 0.3- and 0.6-taper-ratio wings are in the presence of the basic and indented bodies, except where otherwise noted.

Effect of wing normal-force coefficient.- With increases in the wing normal-force coefficient at constant Mach number (figs. 7 to 10), the slopes of the angle-of-attack, pitching-moment-coefficient, and bending-moment-coefficient curves experience no abrupt changes up to the pitch-up wing normal-force coefficient. It is noteworthy that all the force- and moment-coefficient curves exhibited some change in slope at this pitch-up wing normal-force coefficient. Further increases in the wing normal-force coefficient generally caused additional changes in the slopes of these curves.

Effect of Mach number.- With increases in Mach number from 0.60 to approximately 0.95, the slopes of the wing-normal-force-coefficient curves increased significantly in the low wing-normal-force-coefficient range (figs. 7(a), 8(a), 9(a), and 10(a)). Further increases in Mach number to the maximum tested caused gradual decreases in the slopes.

Mach number increases from 0.60 to the maximum tested caused increases in the slopes of that portion of the pitching-moment curves below the pitch-up wing normal-force coefficient (figs. 7(b), 8(b), 9(b), and 10(b)). The pitch-up wing normal-force coefficient increases from approximately 0.4 to 0.7 with increases in Mach number from 0.60 to 1.20.

The slopes of the bending-moment-coefficient curves increase gradually with increases in Mach number from 0.60 to 1.20 in the low range of the wing normal-force coefficient (figs. 7(c), 8(c), 9(c), and 10(c)).

Longitudinal and lateral locations of the center of pressure.- The effects of wing normal-force coefficient, taper ratio, and Mach number on the longitudinal and lateral location of the center of pressure for the wings are shown in figures 11 and 12. The rapid forward and inboard movements of the center of pressure for values of wing normal-force coefficients between approximately 0.4 and 0.7 (figs. 11(a) and 12(a)) are associated with pitch-up. (See figs. 7(b), 8(b), 9(b), and 10(b).) Before pitch-up occurs, there is generally a rearward movement of the center of pressure of the order of 4 percent of the mean aerodynamic chord and relatively little lateral movement for a constant Mach number.

With increases in Mach number from approximately 0.60 to 0.85 at a constant wing normal-force coefficient below pitch-up, the longitudinal and the lateral locations of the center of pressure experience no appreciable movement (figs. 11(b) and 12(b)). Between Mach numbers of 0.85 and 1.0, the onset of supersonic flow over the wing produced a major change in both the longitudinal and lateral locations of the center of pressure for both wings. Rearward movements of the order of 15 percent of the mean aerodynamic chord in conjunction with outboard shifts of the order of 5 percent of the wing semispan were experienced. Above Mach number 1.0, the longitudinal center-of-pressure locations experienced additional rearward movements at a reduced rate, whereas the lateral locations remained essentially constant.

The center-of-pressure loci (figs. 13 and 14) show the combined longitudinal and lateral center-of-pressure movements throughout the range of Mach number and wing normal-force coefficient tested. It should be emphasized here that the accuracy of the data presented does not justify the large plotting scale used in figures 13 and 14. This large scale was chosen to separate the data sufficiently to allow the effects of Mach number and wing normal-force coefficient to be evident and distinct, in addition to presenting the longitudinal and lateral movements in the proper proportion to each other. An important point to note is that the center-of-pressure movement occurs within the same general boundaries for all the configurations. Also of interest is the fact that although the center of pressure moves generally forward with respect to a fixed point on the wing with increase in wing normal-force coefficient, it is actually moving rearward with respect to the local chord at the lateral position of the center of pressure. The mean aerodynamic chord for both the total wing and exposed wing and the quarter-chord line are shown for orientation.

Maximum bending moments.- Analysis of figures 7(c), 8(c), 9(c), 10(c), 11, and 12 shows that the maximum bending moments do not occur at the most

outboard location of the center of pressure. These outboard center-of-pressure locations occur at the wing normal-force coefficients up to pitch-up. For a given Mach number, the decrease in the moment arm due to the inboard movement of the center-of-pressure location with increases in the wing normal-force coefficient above pitch-up is more than compensated for by increases in the wing normal force. Consequently, the wing bending moment continues to increase as the center-of-pressure location moves inboard.

Division of load between the wing and body.- The division of normal-force and pitching-moment load between the wing and body is shown in figures 15 and 16.

Figure 15 shows the division of normal-force load as total normal-force coefficient against normal-force coefficient for the wing in the presence of the body. Also shown in figure 15 is the difference between the total normal-force coefficient and the wing normal-force coefficient. This difference is the normal-force coefficient for the body plus wing interference. In general, the normal-force load carried by the body is less than the ratio of wing area blanketed by the body to the total wing area would indicate ( $\frac{S - S_e}{S}$  line on fig. 15). Reference 6 points out that this simple area ratio may approximate the division of normal-force load under certain conditions. However, there are theoretical methods which give closer prediction. A slight Mach number effect on the division of normal-force load for the basic body configurations is apparent. This effect was diminished considerably by body indentation.

Figure 16 shows the division of pitching-moment load as pitching-moment coefficient for the wing-body combination and for the wing in the presence of the body against wing-body normal-force coefficient. For all the configurations, the pitching-moment curves for the wing in the presence of the body are very similar in shape up to pitch-up to the pitching-moment curves for the wing-body combination except for a considerably more negative slope. Both the wing-body combination and the wing in the presence of the body experience pitch-up at approximately the same normal-force coefficient. However, the wing-body combination exhibits more exaggerated pitch-up characteristics because of the influence of the large positive pitching moment of the body in this normal-force-coefficient range.

#### Effect of Taper Ratio

At a constant Mach number, an increase in taper ratio increased the wing normal-force coefficient where pitch-up occurs (figs. 7(b), 8(b), 9(b), and 10(b)). Therefore, the rapid forward and inboard movement of the center of pressure associated with pitch-up is delayed to a higher

wing normal-force coefficient for the higher taper-ratio wing (figs. 11(a) and 12(a)).

As previously mentioned, the onset of supersonic flow over the wings between a Mach number of 0.85 and 1.0 causes a rapid rearward and outboard movement of the center of pressure (figs. 11(b) and 12(b)). The increase in taper ratio from 0.3 to 0.6 delays slightly the Mach number where this rearward and outboard movement begins.

Examination of figures 11 and 12 indicates that increases in taper ratio from 0.3 to 0.6 cause the longitudinal center-of-pressure location to move forward as much as 11 percent of the mean aerodynamic chord. It should be emphasized that the major portion of these differences can be attributed directly to the differences in the length and spanwise location of the mean aerodynamic chords of the two wings. Better correlation between the data for the two wings can be obtained by utilizing the average chord as a reference since it is the same length and at the same spanwise location for both wings. A plot showing a comparison in this form is presented in figure 17 to show the effect of taper ratio, wing normal-force coefficient, and Mach number. Since the correlation is much improved over the results using  $\bar{c}$  as a reference (figs. 11 and 12), it is apparent that the increases in taper ratio from 0.3 to 0.6 had little effect on the longitudinal location of the center of pressure below pitch-up when using the average chord as a reference. Differences of a maximum of only 4 percent were noted in the transonic Mach number range. The delay, due to an increase in taper ratio, in the normal-force coefficient at which the forward movement of the location of the center of pressure associated with pitch-up begins is more evident in figure 17 than in figures 11 and 12. Another effect of the increase in taper ratio which is more evident than before is the slight delay in the Mach number at which the rapid rearward movement of the center of pressure begins (fig. 17(b)).

In an attempt to improve further the correlation, other parameters were utilized, including replacing  $C_{N_W}$  with a normal-force coefficient based on the exposed wing area. However, no substantial further improvement in the correlation of the longitudinal location of the center of pressure was obtained.

In summarizing, the effects of taper ratio on the longitudinal and lateral locations of the center of pressure are rather small. Below pitch-up the increase in taper ratio was accountable for a maximum difference in the longitudinal locations of 4 percent of the average chord and a maximum difference in the lateral locations of 3 percent of the wing semispan.

### Effects of Body Indentation

The effects of body indentation on the longitudinal and lateral locations of the center of pressure are shown in figures 18 and 19. The major effect of body indentation is to delay the Mach number at which the rapid rearward movement of the center of pressure begins (fig. 19). Other effects of body indentation on the loading characteristics are negligible.

### Comparisons With Other Data

The longitudinal and lateral locations of the center of pressure obtained during this investigation are compared with results from a pressure-model investigation (ref. 7) in figure 20. The wing used in the investigation of reference 7 is similar to the 0.6-taper-ratio wing of this investigation. However, the body configurations were different. Two different bodies were utilized and were designated the curved body and the cylindrical body, respectively. The curved body was a fineness-ratio-10 body having a curved profile from the nose to the base. The cylindrical body was a fineness-ratio-11.8 body having a curved profile from the nose to the wing leading edge and a cylindrical section from the wing leading edge to the base of the model. The center-of-pressure locations from the two investigations are in generally good agreement. This agreement indicates that changes in body shape of the nature experienced in these two investigations have no pronounced effects on the center-of-pressure locations.

Calculated lateral locations of the center of pressure in accordance with references 8, 9, and 10 are compared with the experimental values obtained from the basic body configurations during this investigation in figure 21. Reference 8 is applicable at subsonic Mach numbers. Reference 9 is applicable in the supersonic Mach number range from 1.163 and 1.288 for the 0.3- and 0.6-taper-ratio wings, respectively, to approximately 1.5. Reference 10, however, is applicable at lower supersonic Mach numbers for these two wings (approximately 1.02 to 1.5). Since the computations in accordance with reference 10 are very time consuming, this reference was utilized for only two points. Points were computed in accordance with references 8 and 9 for the 0.3-taper-ratio wing (fig. 21(a)) and in accordance with references 8, 9, and 10 for the 0.6-taper-ratio wing. Body interference was not included in the calculations.

The comparison showed generally good agreement. In the transonic speed range the experimental values show a smooth transition from the lateral center-of-pressure position for subsonic speeds to the position for low supersonic speeds. This transition is completed at a Mach number near 1.0. The calculated values for the 0.6-taper-ratio wing (fig. 21(b)) show that both references 9 and 10 give the same result at a Mach number of 1.288; however, reference 10 appears to predict a

transition somewhere between a Mach number of 1.092 and 1.288, which is at a considerably higher Mach number than the experimental transition. The good agreement at moderate supersonic speeds ( $M \approx 1.2$ ) between the calculated and experimental values and the characteristics of the experimental lateral position to stabilize at its supersonic value around a Mach number of 1.0 indicates that the lateral center-of-pressure position at low supersonic speeds could be predicted (below pitch-up) from the values calculated in accordance with reference 9 at the higher Mach number where the theory becomes applicable ( $M \approx 1.2$ ).

### CONCLUSIONS

Results obtained in the Langley 8-foot transonic pressure tunnel to determine the effects of taper ratio and body indentation on the aerodynamic loading characteristics of a  $45^\circ$  sweptback wing in the presence of a body lead to the following conclusions:

1. An increase in taper ratio from 0.3 to 0.6 through the Mach number range from 0.6 to 1.2 with increases in wing normal-force coefficient up to approximately 0.8 results in a delay in the Mach number for the transonic rearward and outboard movement of the center of pressure which causes differences of a maximum of 4 percent of the average chord in longitudinal location and differences of a maximum of 3 percent of the wing semispan in the lateral location below pitch-up. Also, a delay results in the wing normal-force coefficient at which pitch-up occurs.

2. Body indentation delays slightly the Mach number at which the transonic rearward movement of the center of pressure begins. Other effects of body indentation on the loading characteristics are negligible.

3. Good correlation of the effects of taper ratio on the longitudinal center-of-pressure location can be obtained by utilizing the average chord as a reference in lieu of the mean aerodynamic chord.

4. The smooth transition of the center of pressure at transonic speeds and the characteristic of the lateral location to stabilize at its supersonic value around a Mach number of 1.0 allows the lateral location at low supersonic Mach numbers to be predicted from the theoretical value calculated for a higher Mach number.

Langley Aeronautical Laboratory,  
National Advisory Committee for Aeronautics,  
Langley Field, Va., December 10, 1954.

## REFERENCES

1. Whitcomb, Richard T.: A Study of the Zero-Lift Drag-Rise Characteristics of Wing-Body Combinations Near the Speed of Sound. NACA RM L52H08, 1952.
2. Whitcomb, Richard T., and Fischetti, Thomas L.: Development of a Supersonic Area Rule and an Application to the Design of a Wing-Body Combination Having High Lift-to-Drag Ratios. NACA RM L53H31a, 1953.
3. Ritchie, Virgil S.: Effects of Certain Flow Nonuniformities on Lift, Drag, and Pitching Moment for a Transonic-Airplane Model Investigated at a Mach Number of 1.2 in a Nozzle of Circular Cross Section. NACA RM L9E20a, 1949.
4. Morgan, Francis G., and Carmel, Melvin M.: Transonic Wind-Tunnel Investigation of the Effects of Taper Ratio, Body Indentation, Fixed Transition, and Afterbody Shape on the Aerodynamic Characteristics of a 45° Sweptback Wing-Body Combination. NACA RM L54A15, 1954.
5. Osborne, Robert S., and Mugler, John P., Jr.: Effects of Wing Elasticity on the Aerodynamic Characteristics of a 45° Sweptback-Wing-Fuselage Combination Measured in the Langley 8-Foot Transonic Tunnel. NACA RM L52G23, 1952.
6. Gillis, Clarence L.: A Summary of Data on the Division of Loads for Various Wing-Fuselage Combinations. NACA RM L53E08, 1953.
7. Loving, Donald L.: The Effect of a Change in Body Shape on the Loading of a 45° Sweptback Wing-Body Combination at Transonic Speeds. NACA RM L54B09, 1954.
8. DeYoung, John, and Harper, Charles W.: Theoretical Symmetric Span Loading at Subsonic Speeds for Wings Having Arbitrary Plan Form. NACA Rep. 921, 1948.
9. Hannah, Margery E., and Margolis, Kenneth: Span Load Distribution Resulting From Constant Angle of Attack, Steady Rolling Velocity, Steady Pitching Velocity, and Constant Vertical Acceleration for Tapered Sweptback Wings With Streamwise Tips - Subsonic Leading Edges and Supersonic Trailing Edges. NACA TN 2831, 1952.
10. Cohen, Doris: Formulas for the Supersonic Loading, Lift, and Drag of Flat Swept-Back Wings With Leading Edges Behind the Mach Lines. NACA Rep. 1050, 1951.

TABLE I.- BODY COORDINATES

Forebody		Afterbody					
Station, in. from nose	Radius, in.	Basic body		Indented body with 0.3-taper-ratio wing		Indented body with 0.6-taper-ratio wing	
		Station, in. from nose	Radius, in.	Station, in. from nose	Radius, in.	Station, in. from nose	Radius in.
0	0	22.500	1.875	22.500	1.875	22.500	1.875
.225	.104	26.500	1.875	23.380	1.875	23.100	1.875
.5625	.193	27.692	1.868	23.692	1.863	23.625	1.864
1.125	.325	28.692	1.862	24.692	1.819	24.625	1.812
2.250	.542	29.692	1.849	25.692	1.749	25.625	1.742
3.375	.726	30.692	1.825	26.692	1.662	26.625	1.650
4.500	.887	31.692	1.789	27.692	1.579	27.625	1.595
6.750	1.167	32.692	1.745	28.692	1.505	28.625	1.551
9.000	1.390	33.692	1.694	29.692	1.468	29.625	1.537
11.250	1.559	34.692	1.638	30.692	1.469	30.625	1.537
13.500	1.683	35.692	1.570	31.692	1.490	31.625	1.530
15.750	1.770	36.692	1.486	32.692	1.505	32.625	1.499
18.000	1.828	36.900	1.468	33.692	1.506	33.625	1.472
20.250	1.864	37.500	1.408	34.692	1.502	34.625	1.468
		38.500	1.298	35.692	1.491	35.625	1.468
		39.500	1.167	36.692	1.471	36.625	1.468
		40.500	1.030	36.900	1.468	36.900	1.468
		41.250	.937	36.900 to 41.250	(a)	36.900 to 41.250	(a)

<sup>a</sup>Same as basic body coordinates

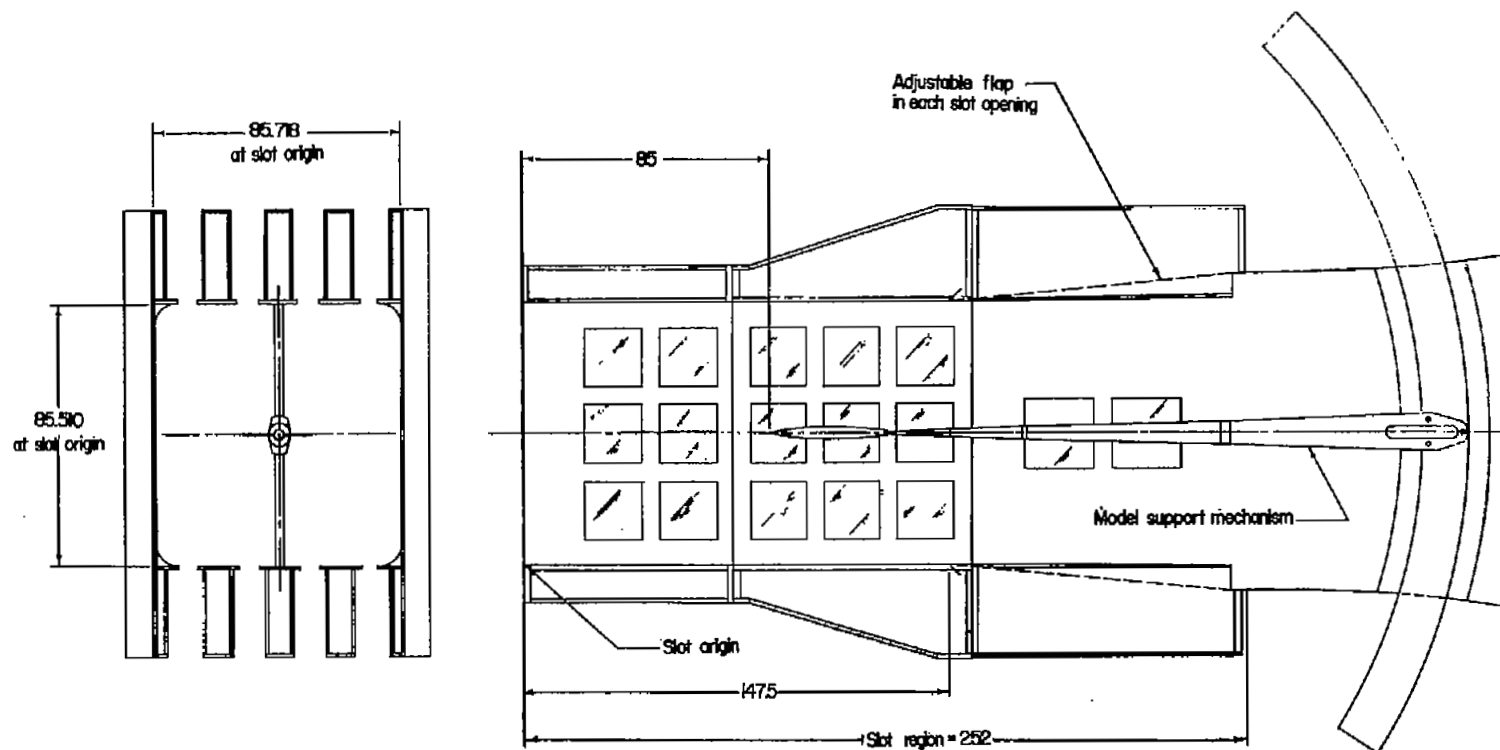


Figure 1.- Details of test section and location of model in the Langley 8-foot transonic pressure tunnel. All dimensions are in inches.

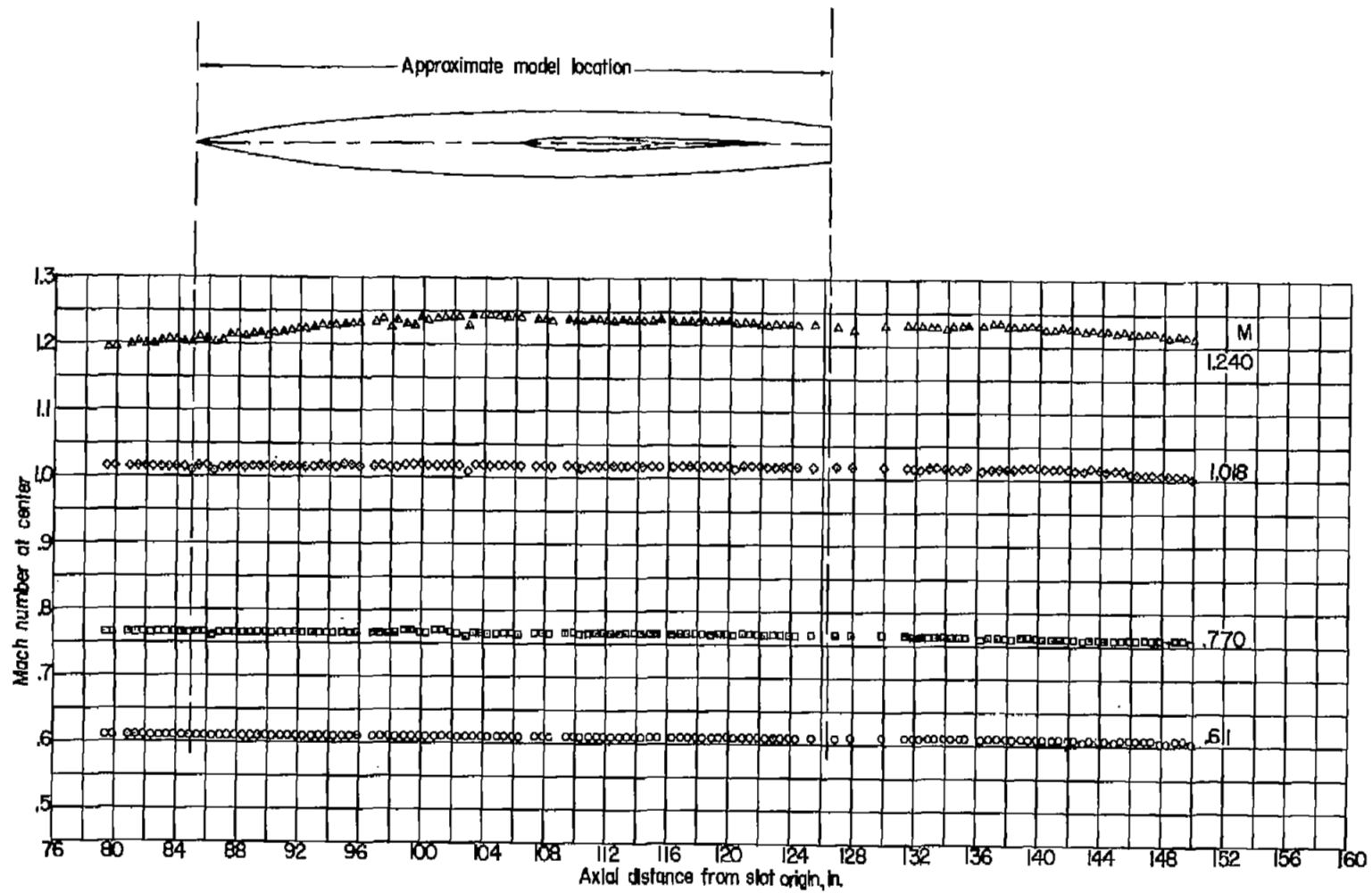
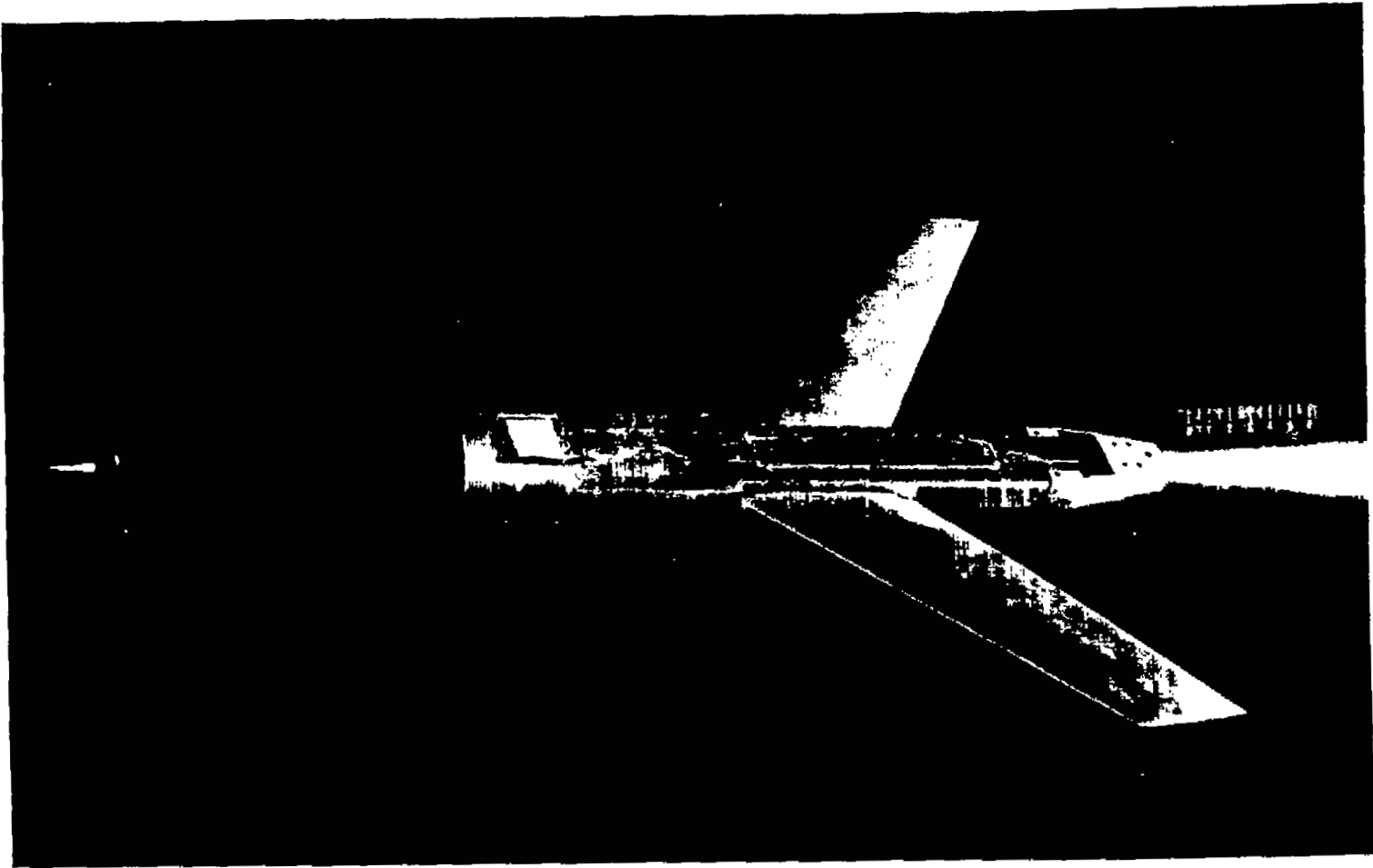
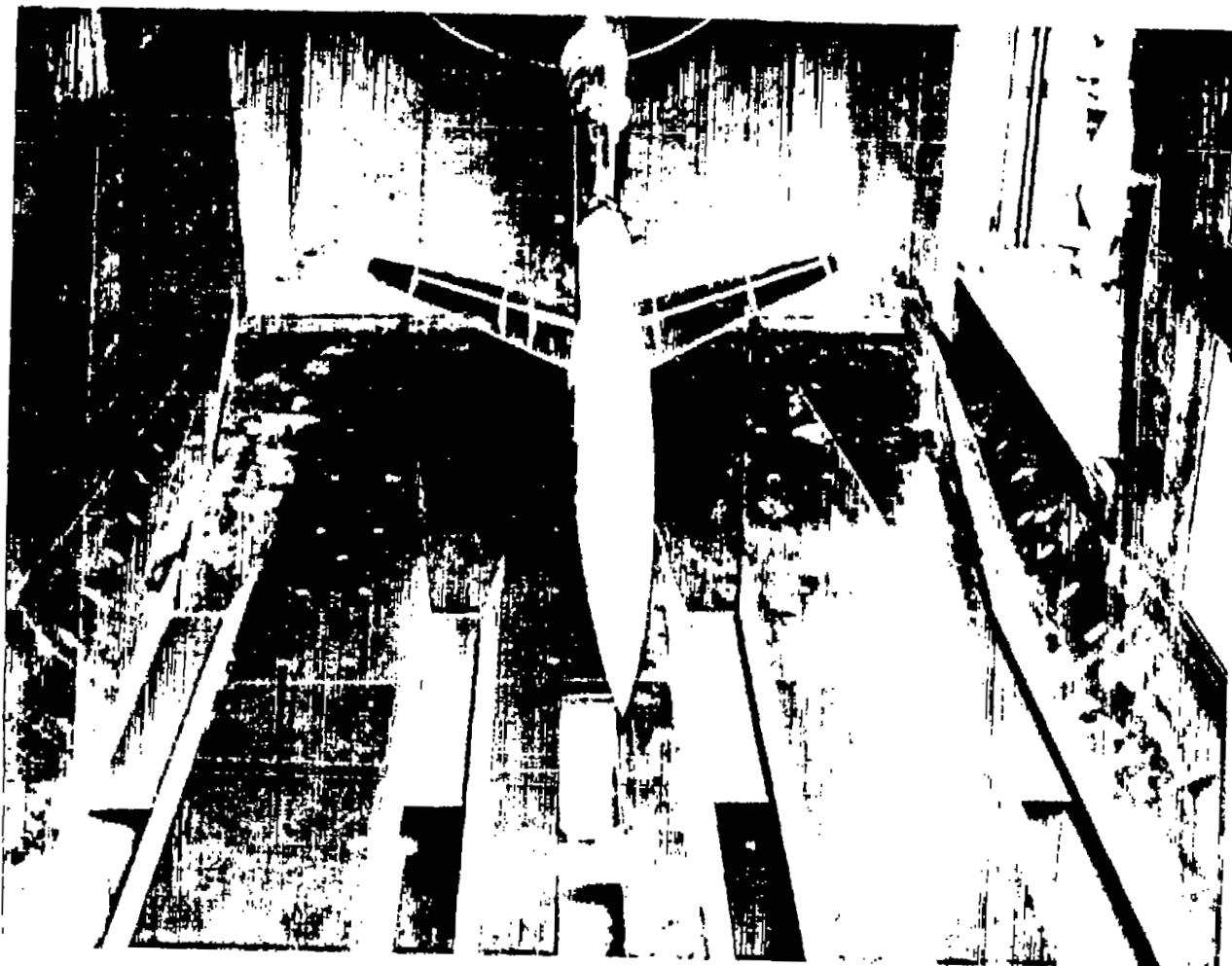


Figure 2.- Typical Mach number distributions in the test section of the Langley 8-foot transonic pressure tunnel during this investigation.



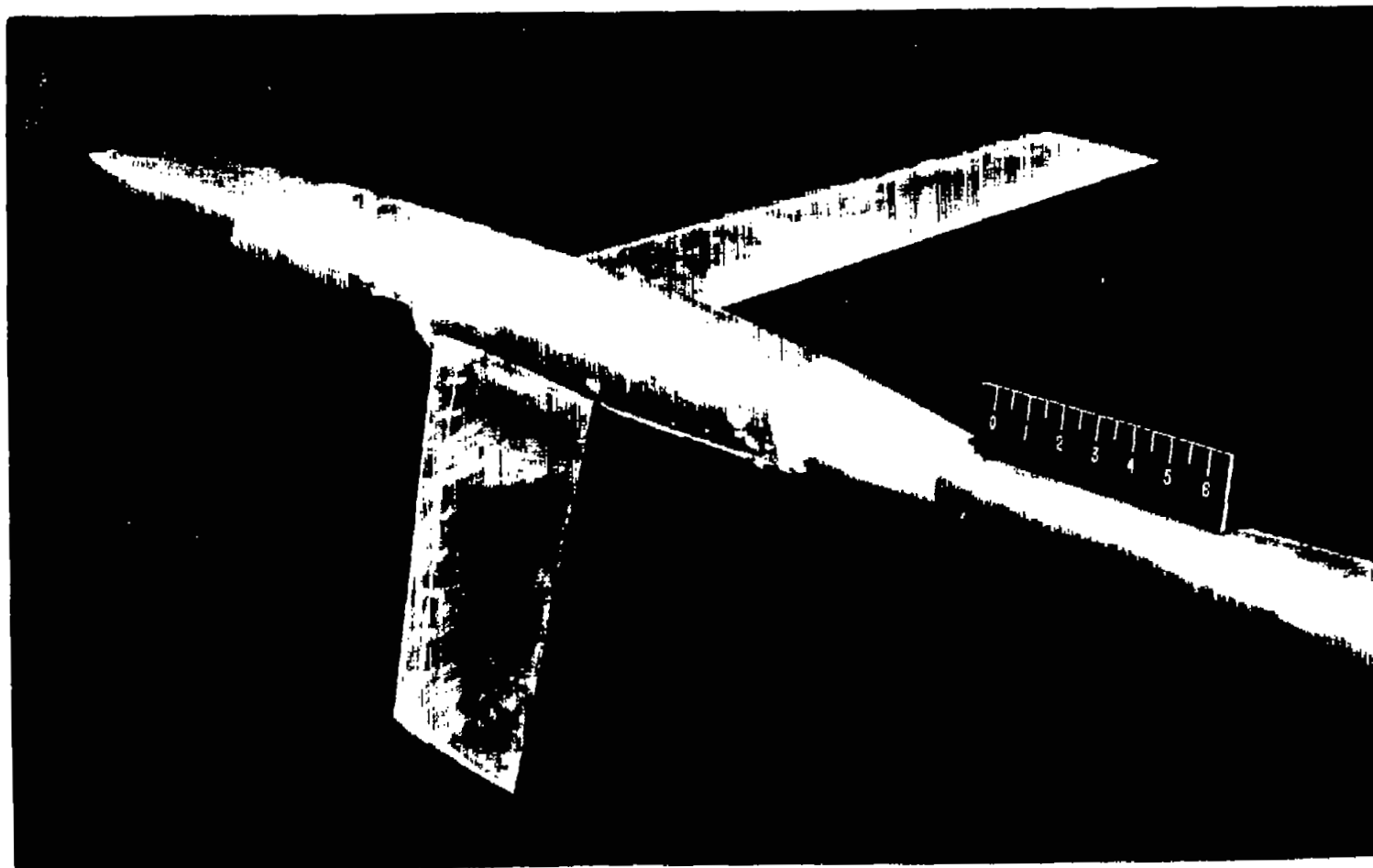
L-84808  
Figure 3.- Model showing balance and wing installed in the body.



(a) 0.3-taper-ratio wing. Indented body.

L-82859

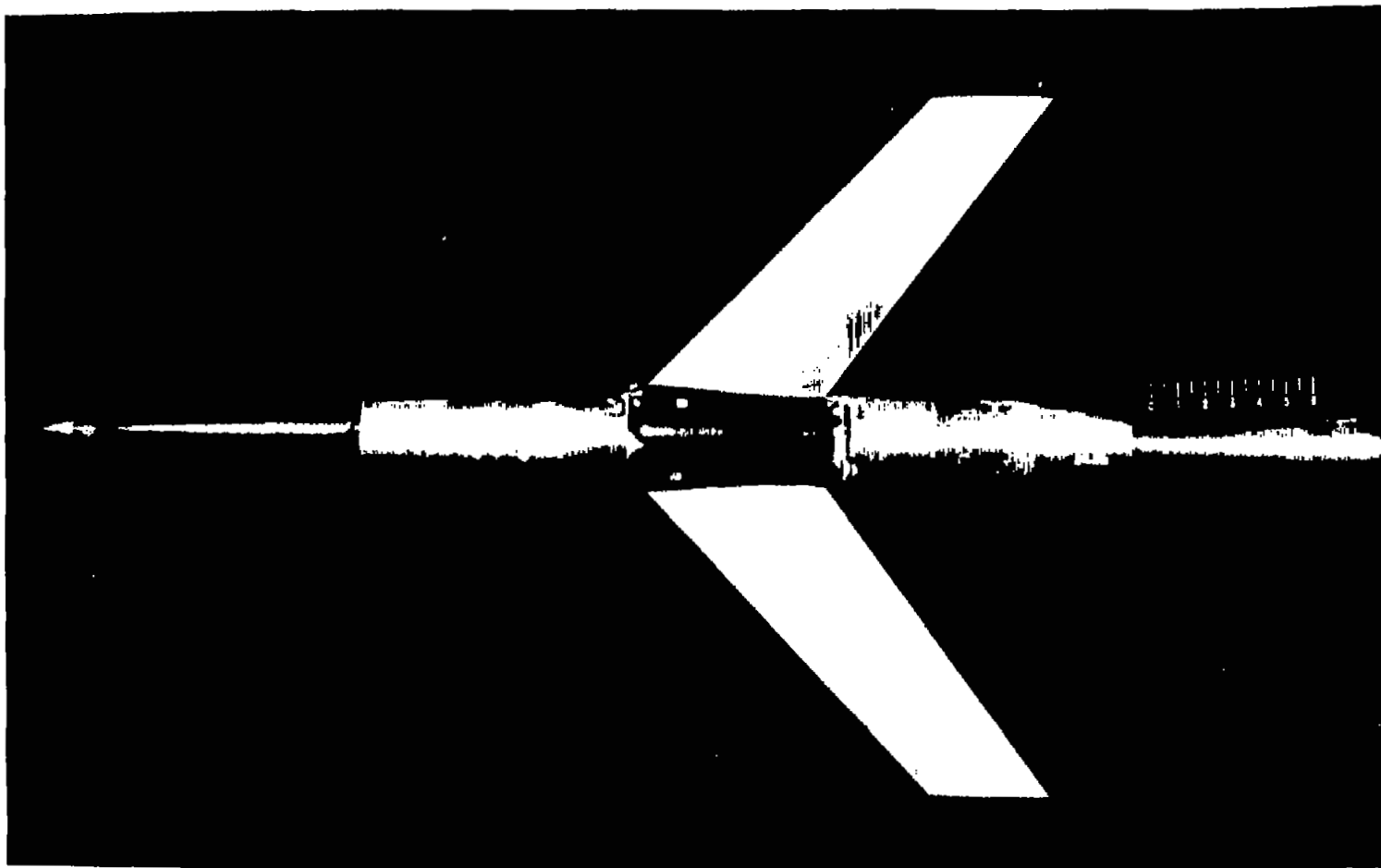
Figure 4.- Typical models tested in the Langley 8-foot transonic pressure tunnel during this investigation.



(b) 0.6-taper-ratio wing. Basic body.

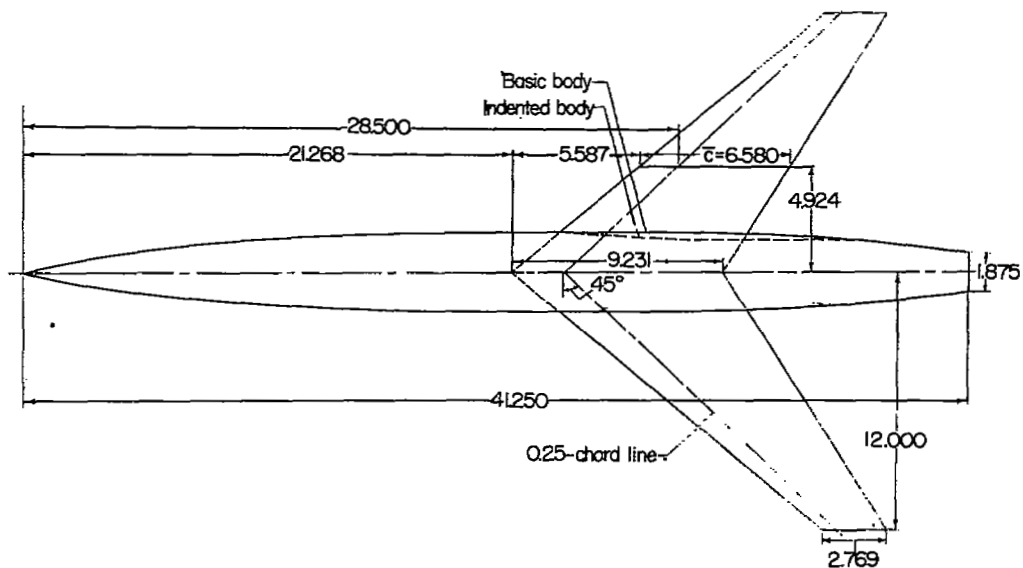
L-84821

Figure 4.- Continued.

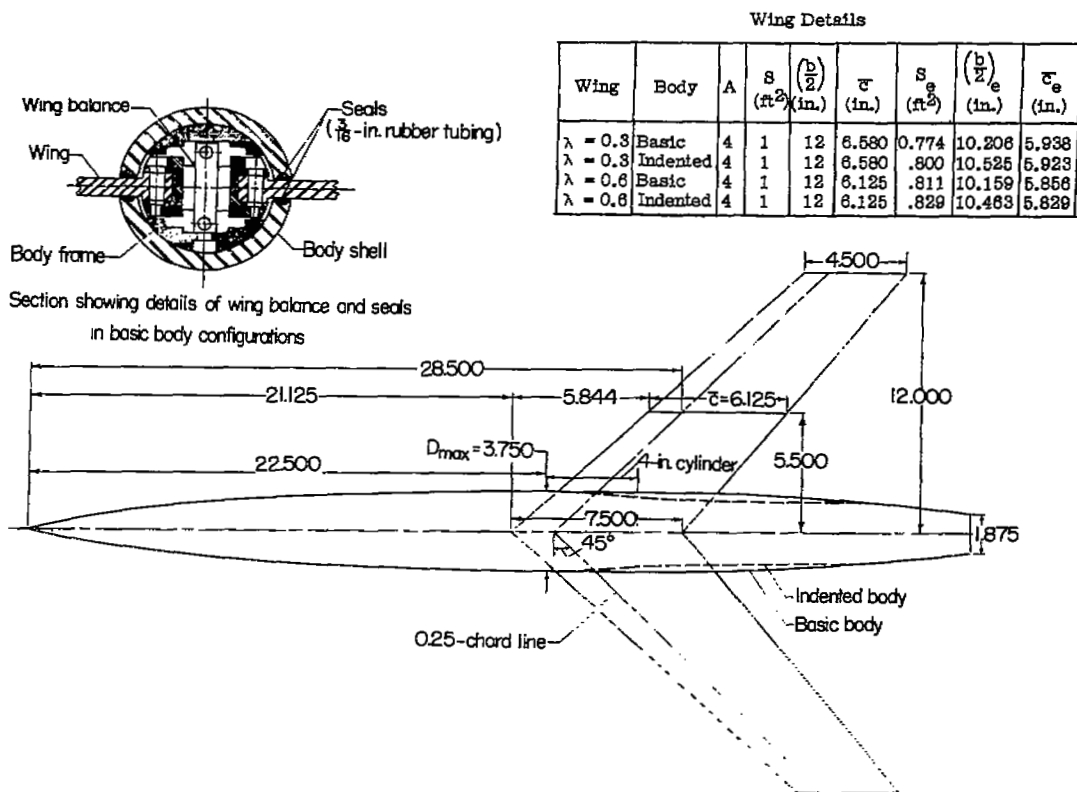


(c) 0.6-taper-ratio wing. Indented body. L-84812

Figure 4.- Concluded.



(a) Wing-body configuration with taper ratio of 0.3.



(b) Wing-body configuration with taper ratio of 0.6.

Figure 5.- Wing-body configurations used in investigation. All dimensions are in inches.

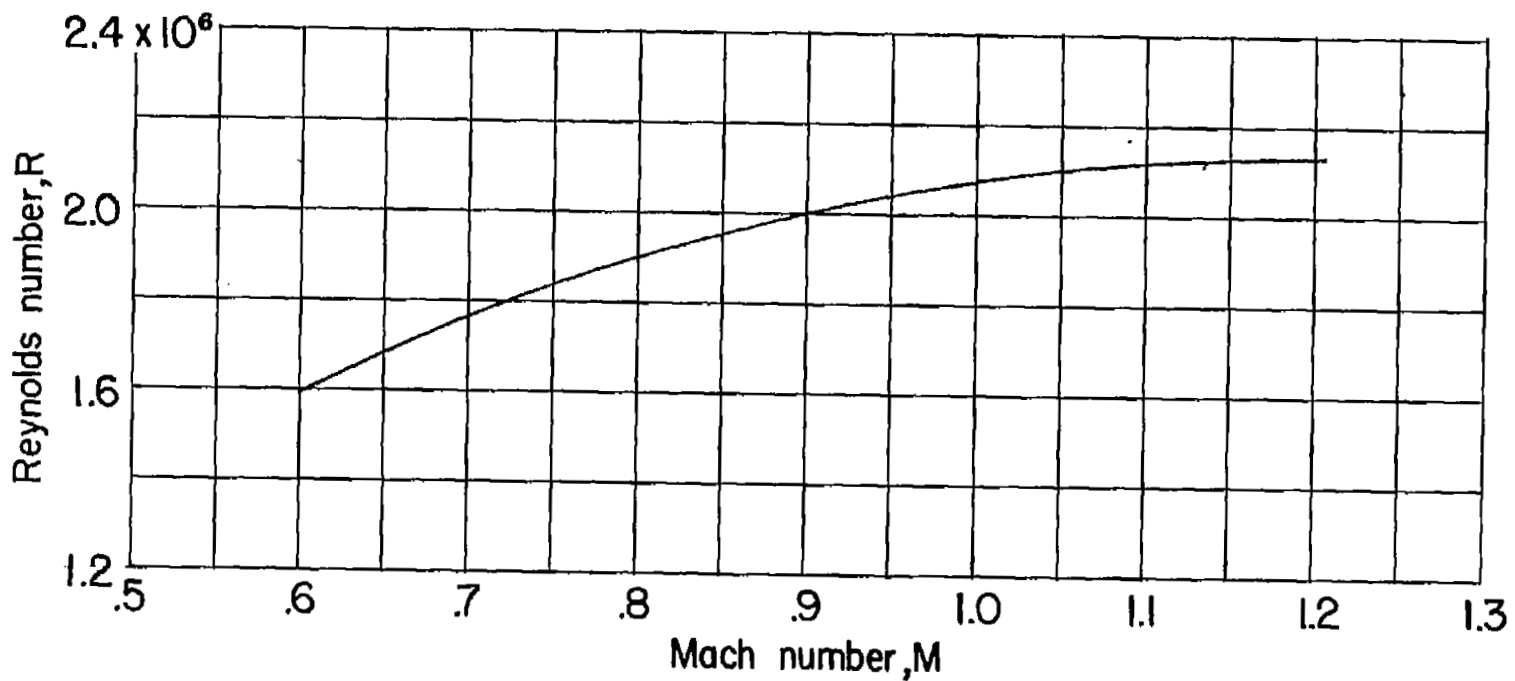
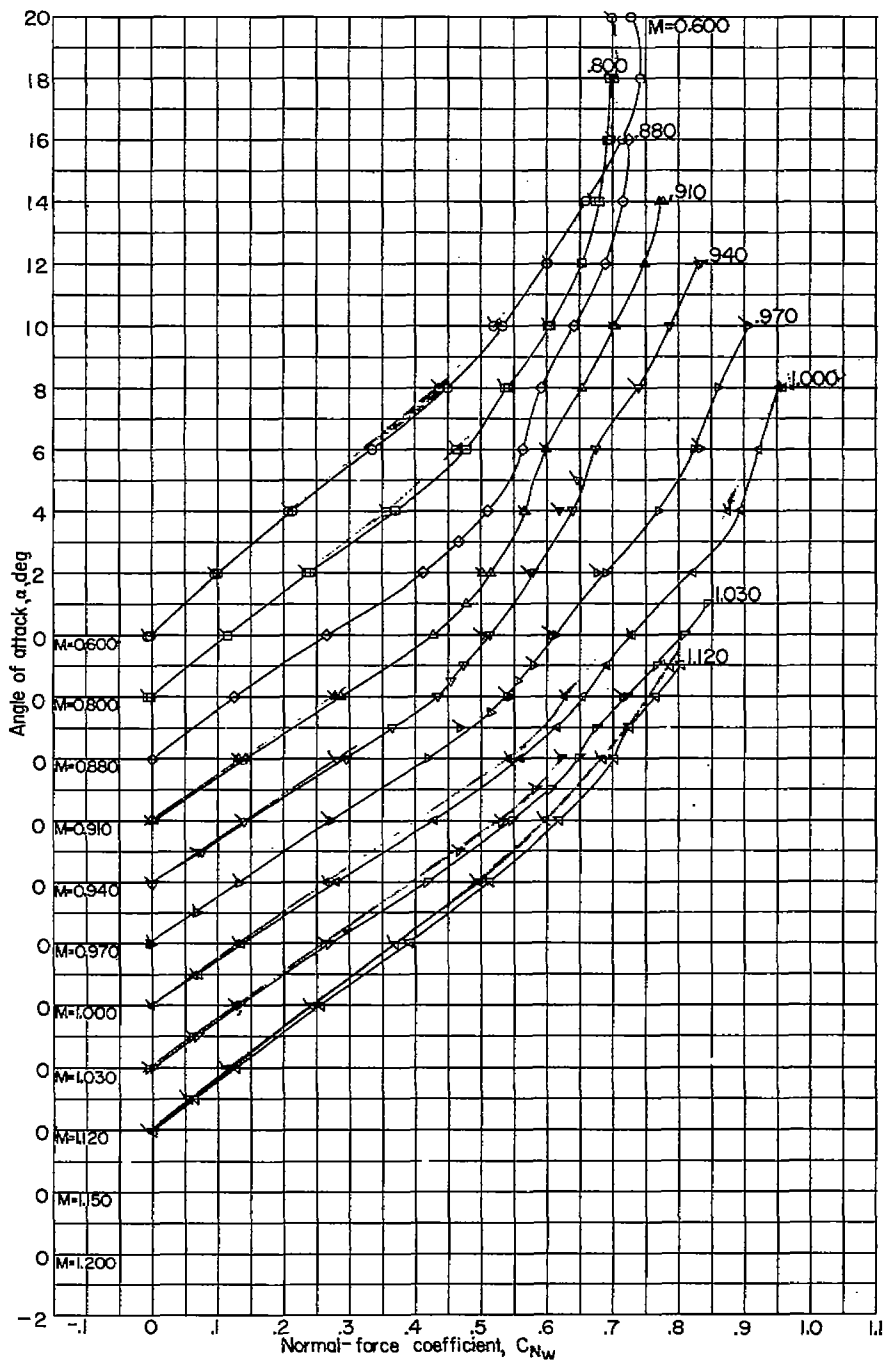
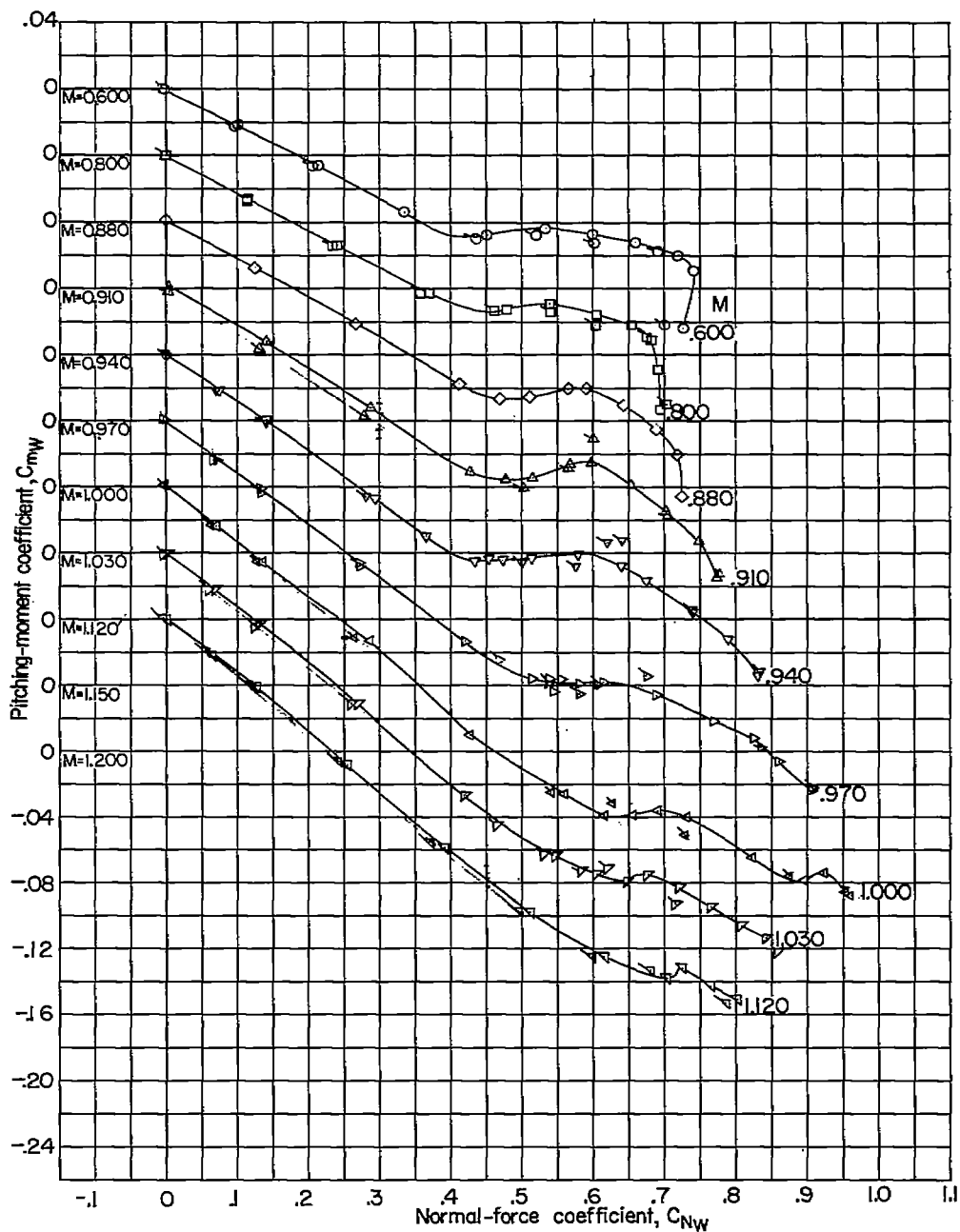


Figure 6.- Typical variation with Mach number of Reynolds number based on wing average chord.



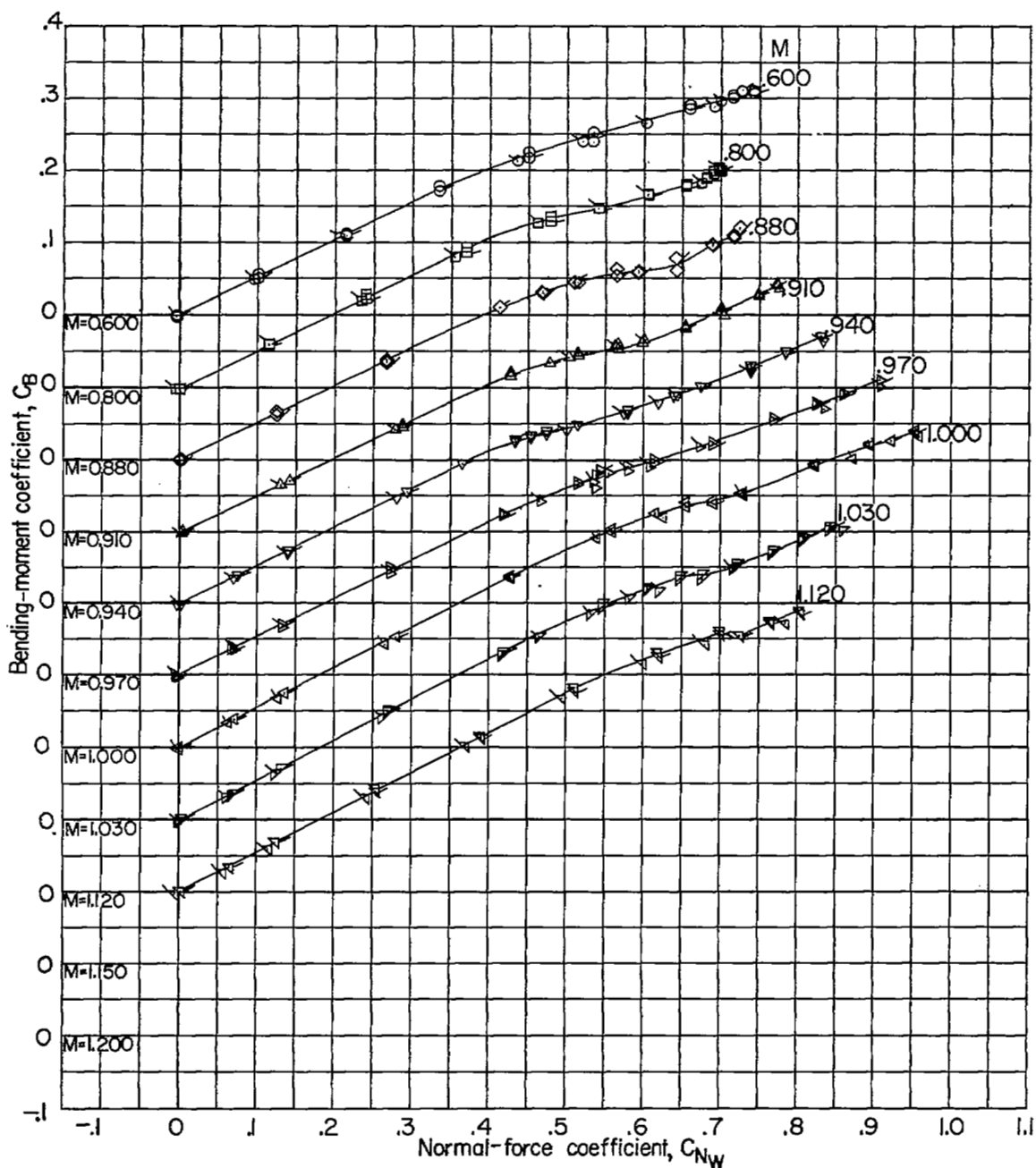
(a) Angle of attack. Plain symbols denote configuration with seals data; symbols flagged left, without seals data.

Figure 7.- Aerodynamic characteristics of the 0.3-taper-ratio wing.  
Basic body.



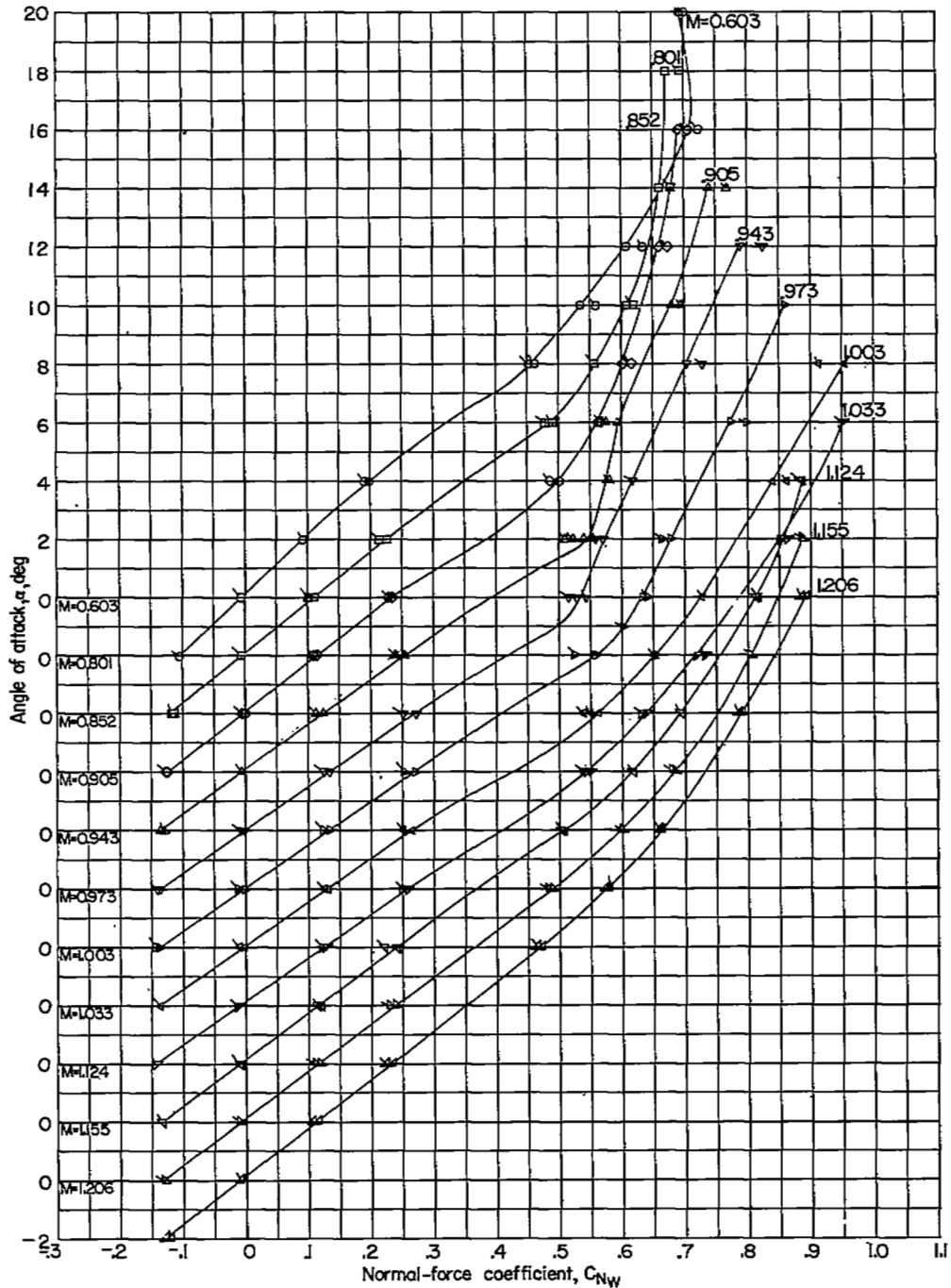
(b) Pitching-moment coefficient. Plain symbols denote configuration with seals data; symbols flagged left, without seals data.

Figure 7.- Continued.



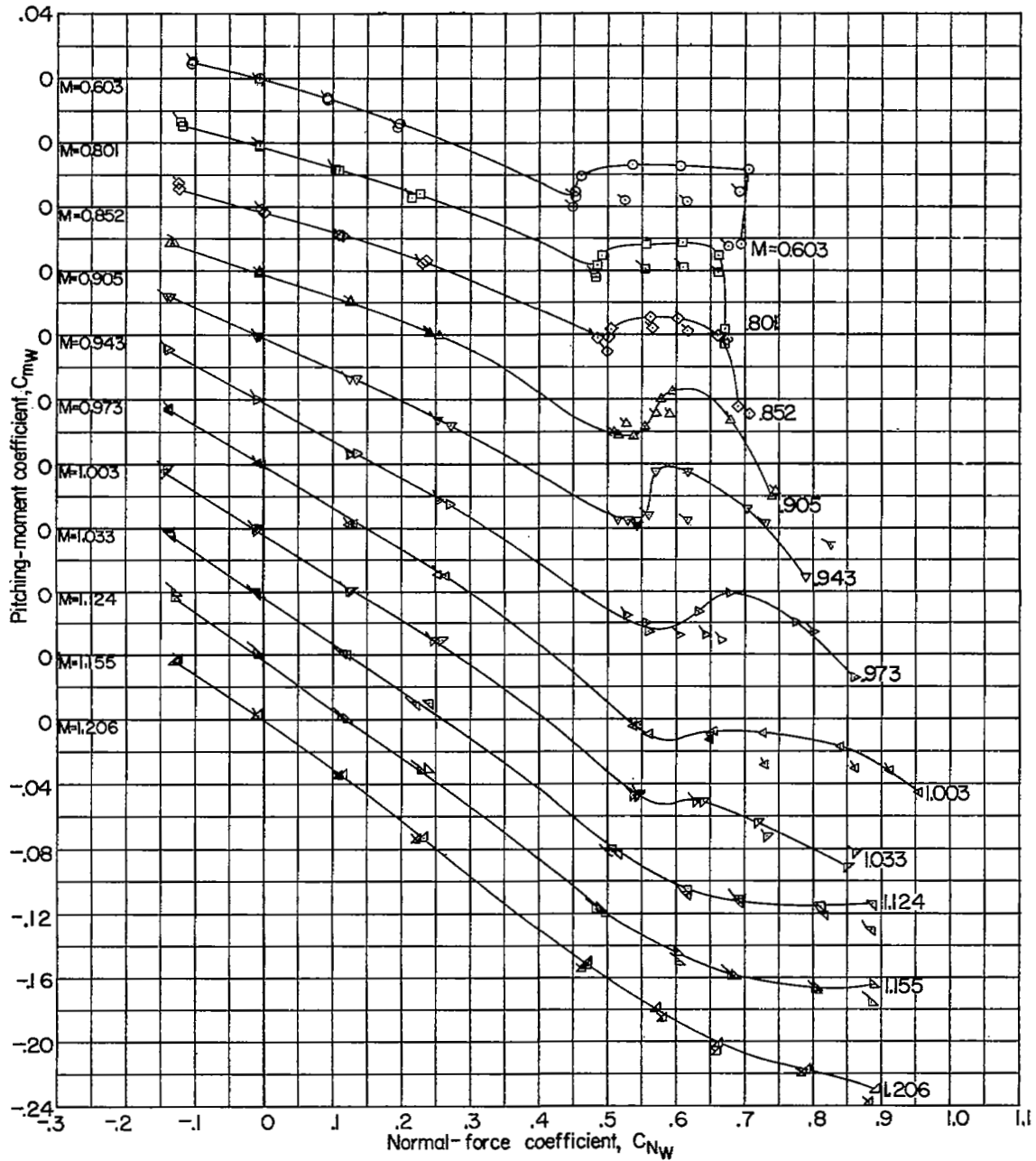
(c) Bending-moment coefficient. Plain and flagged-right symbols denote configuration with seals data for right and left wings, respectively. Symbols flagged left denote the average value of the right and left wings without seals.

Figure 7.- Concluded.



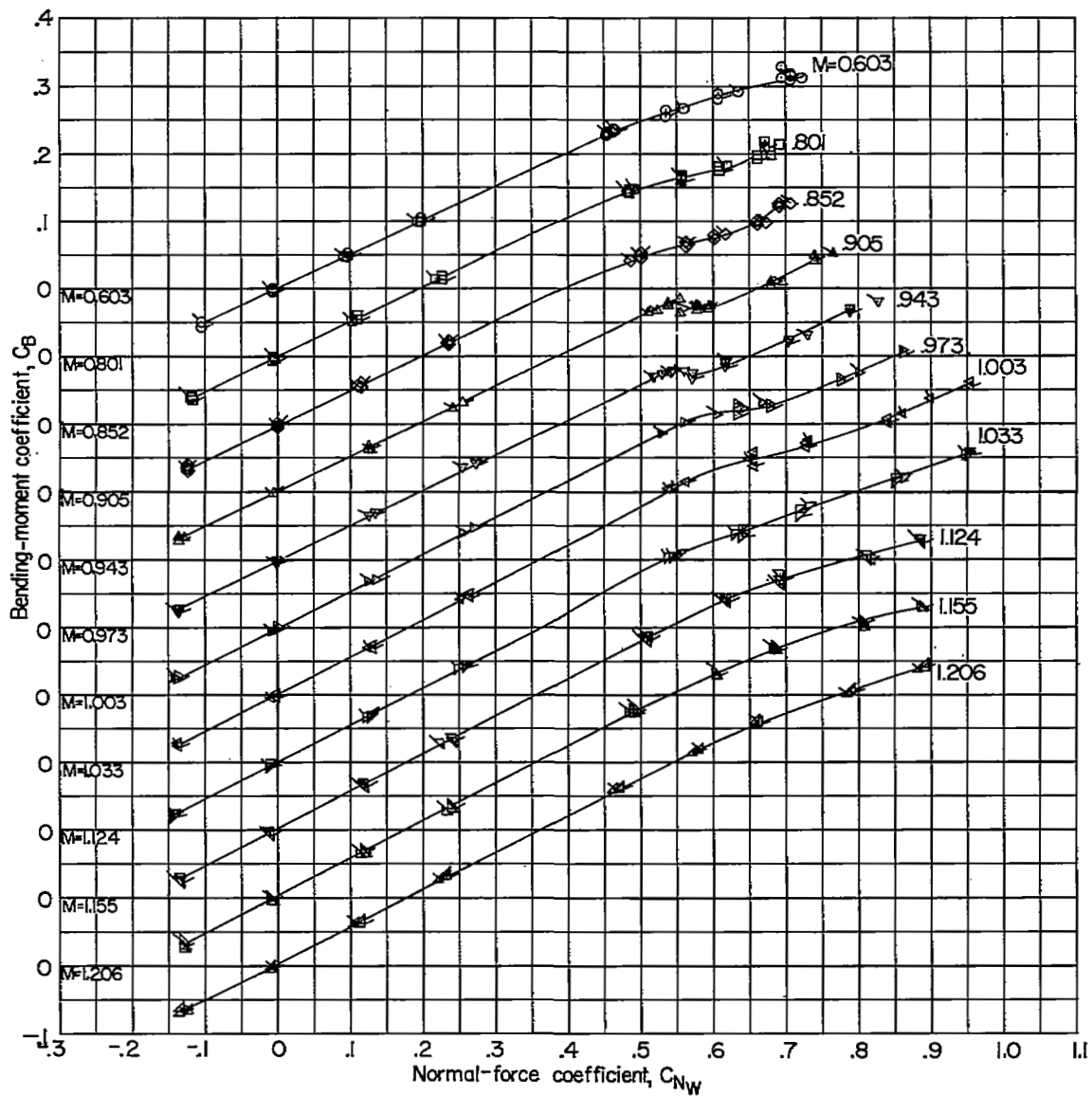
(a) Angle of attack. Plain symbols denote configuration with seals data; symbols flagged left, without seals data.

Figure 8.- Aerodynamic characteristics of the 0.6-taper-ratio wing. Basic body.



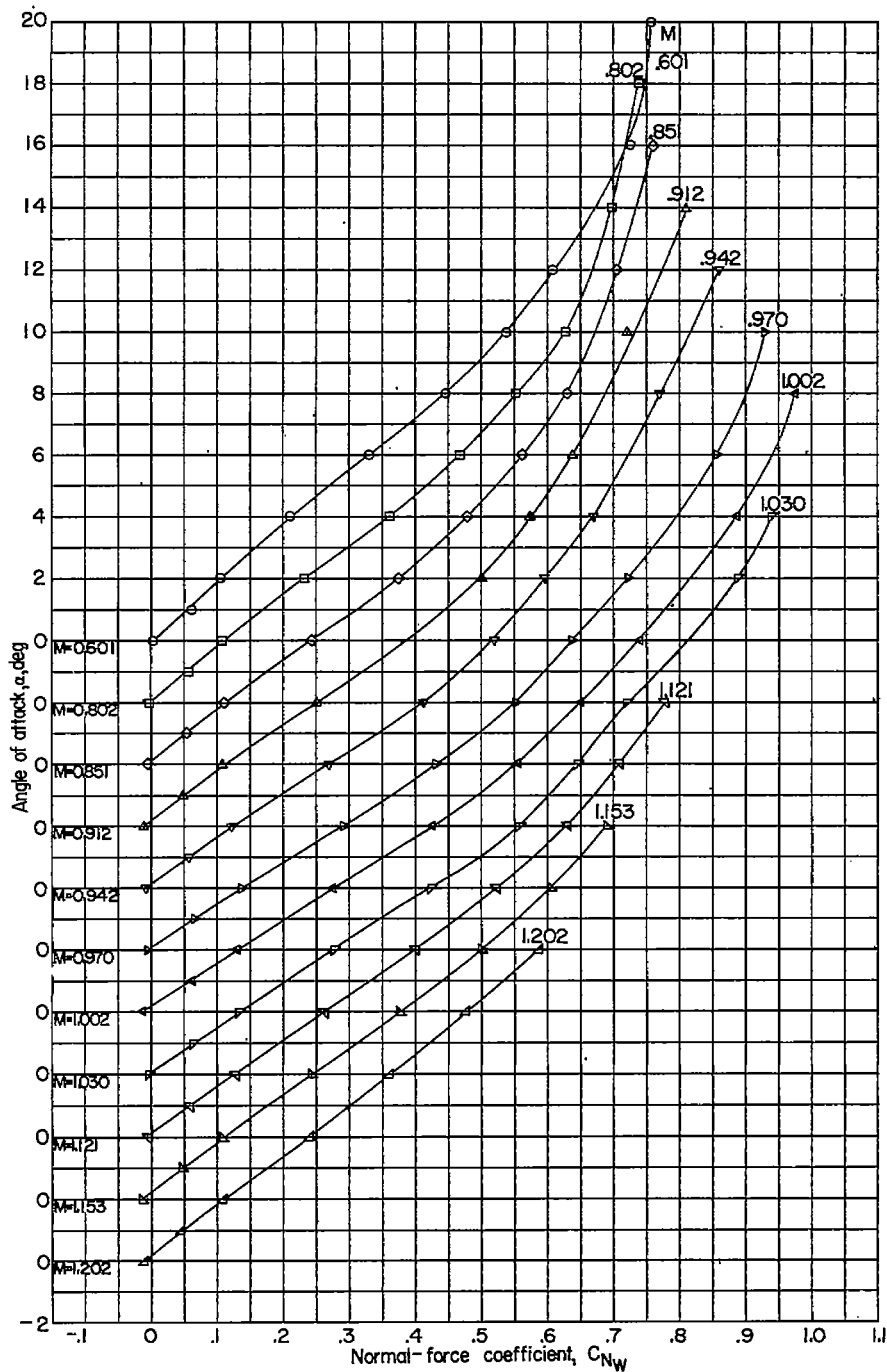
(b) Pitching-moment coefficient. Plain symbols denote configuration with seals data; symbols flagged left, without seals data.

Figure 8.- Continued.



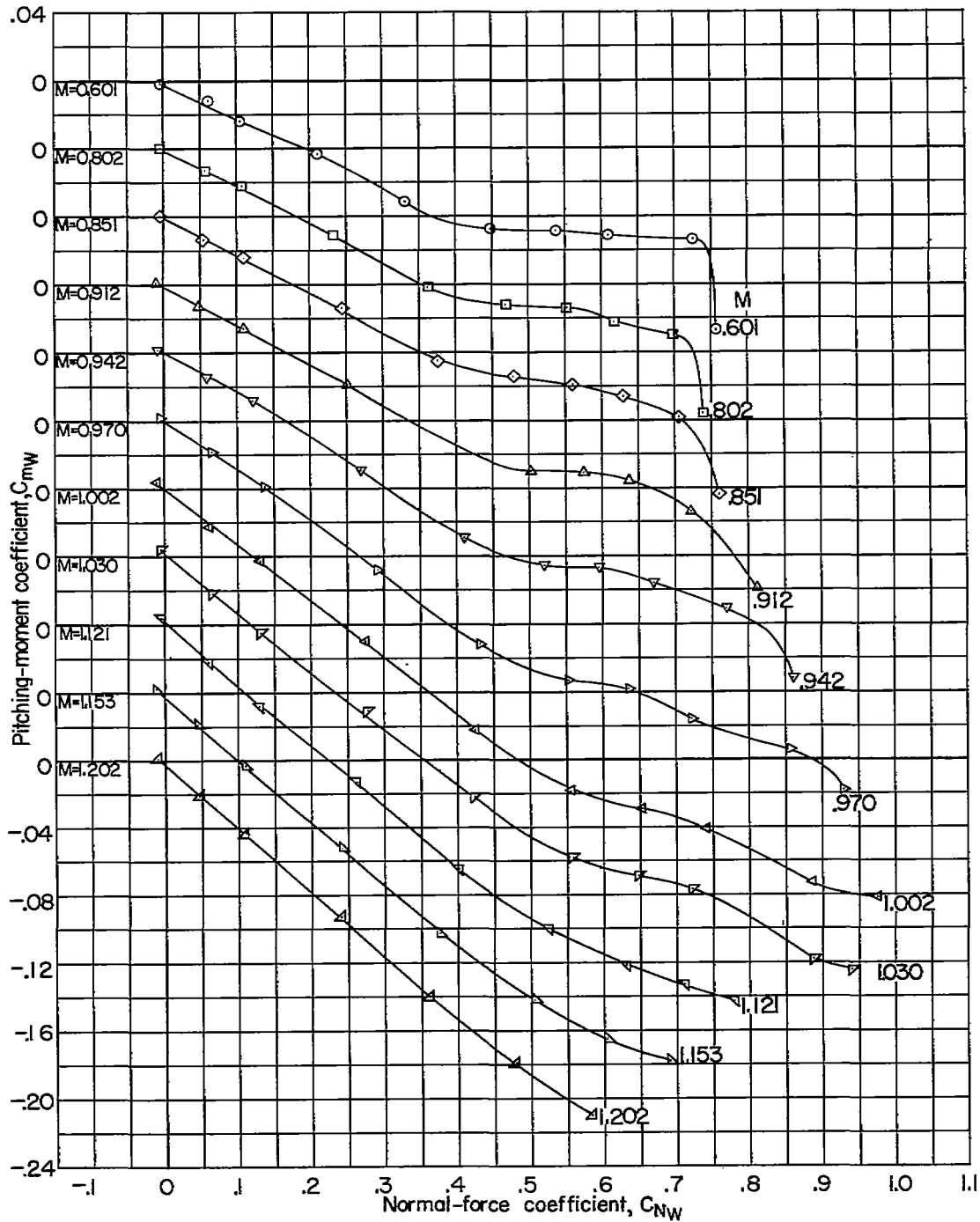
(c) Bending-moment coefficient. Plain and flagged-right symbols denote configuration with seals data for right and left wings, respectively. Symbols flagged left denote the average value of the right and left wings without seals.

Figure 8.- Concluded.



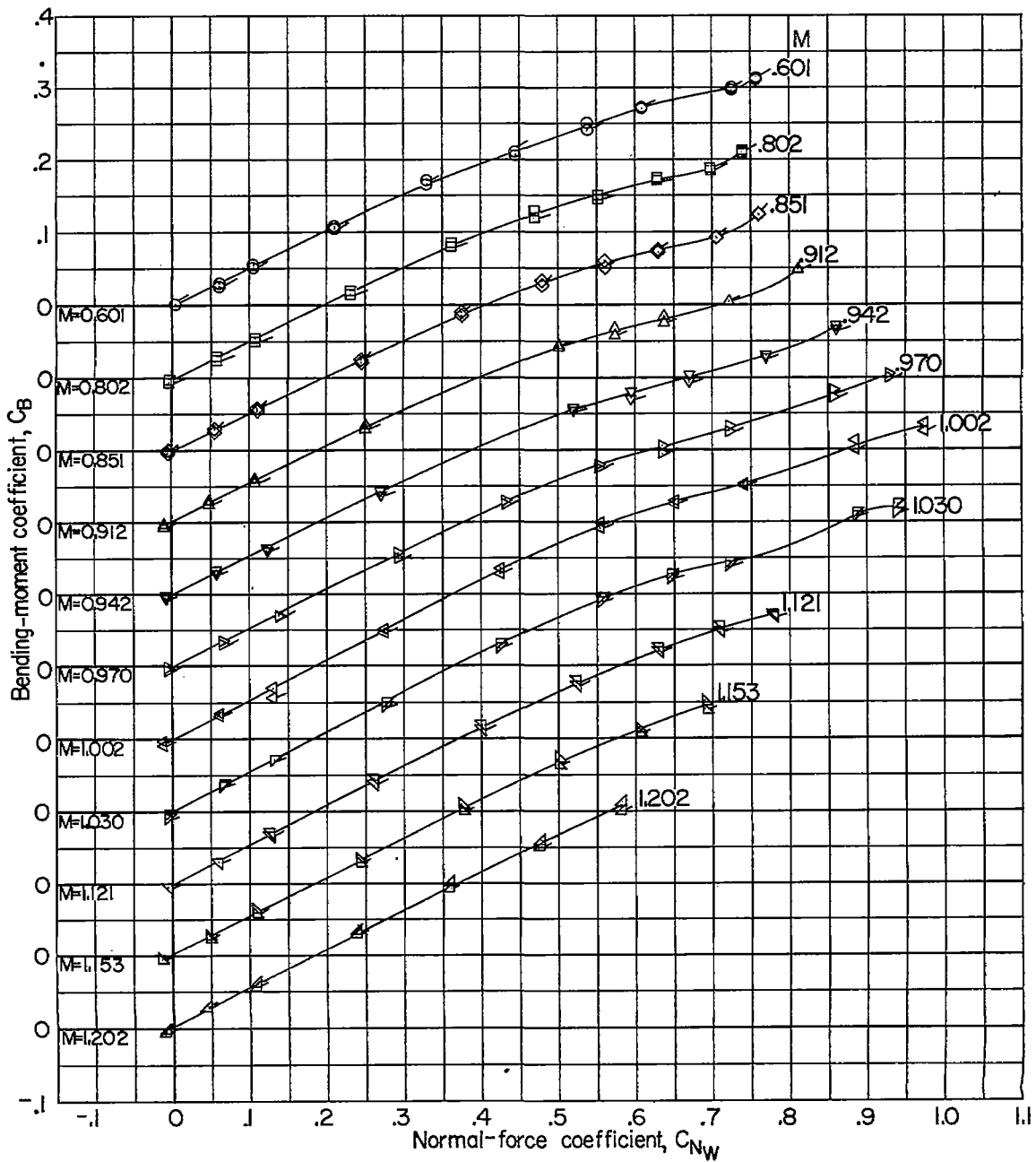
(a) Angle of attack.

Figure 9.- Aerodynamic characteristics of the 0.3-taper-ratio wing. Indented body.



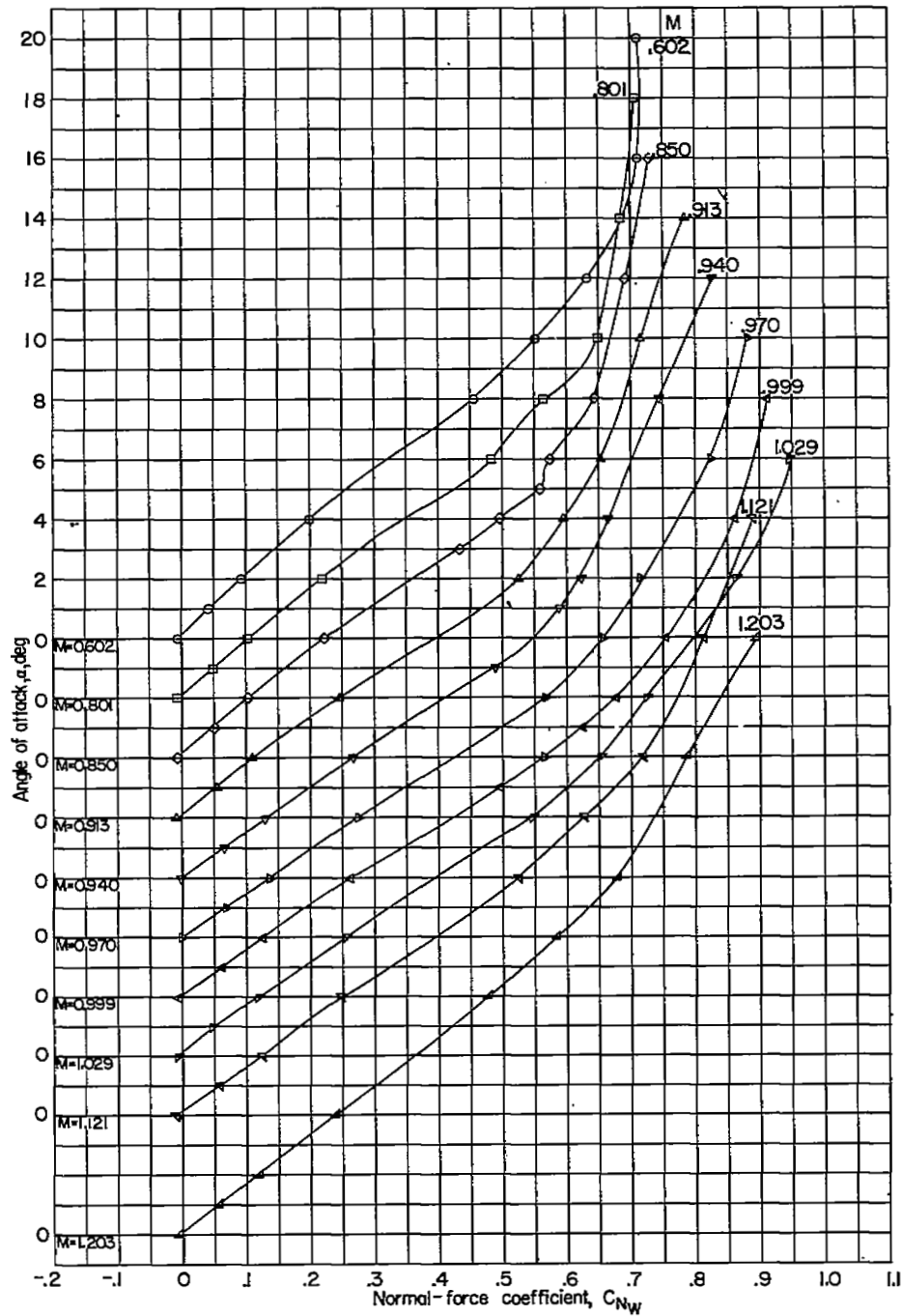
(b) Pitching-moment coefficient.

Figure 9.- Continued.



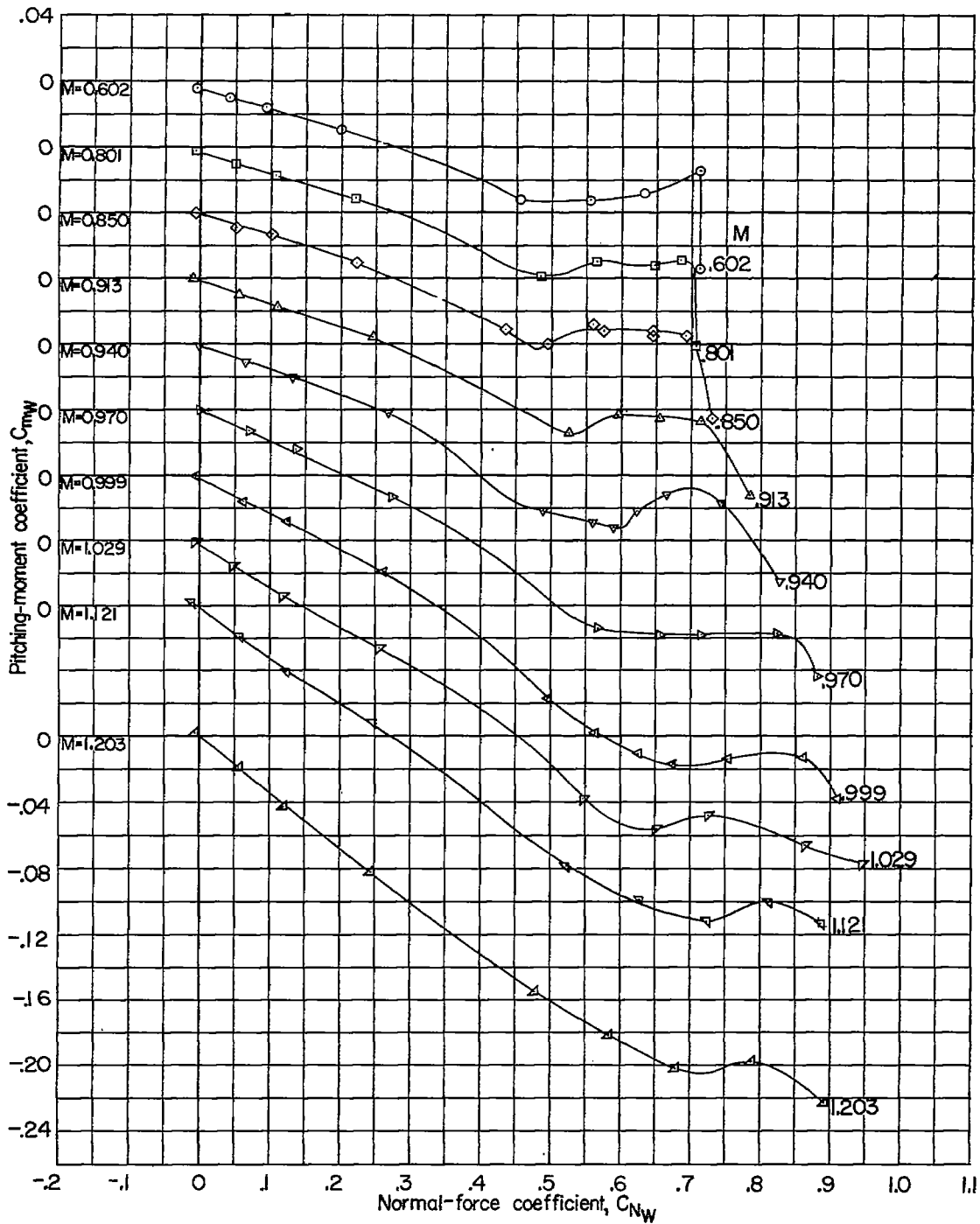
(c) Bending-moment coefficient. Plain and flagged-right symbols denote data for right and left wings, respectively.

Figure 9.- Concluded.



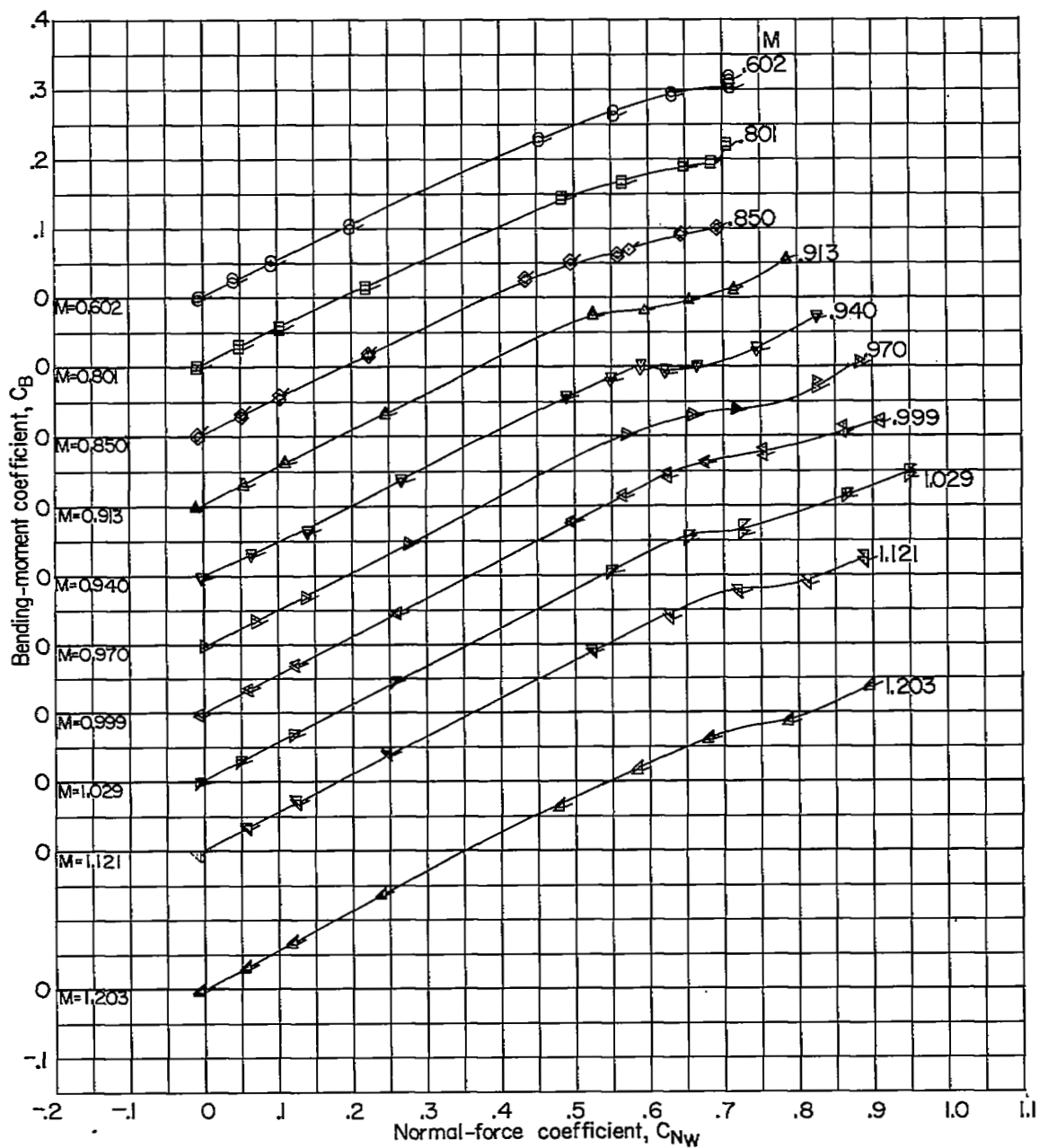
(a) Angle of attack.

Figure 10.- Aerodynamic characteristics of the 0.6-taper-ratio wing.  
Indented body.



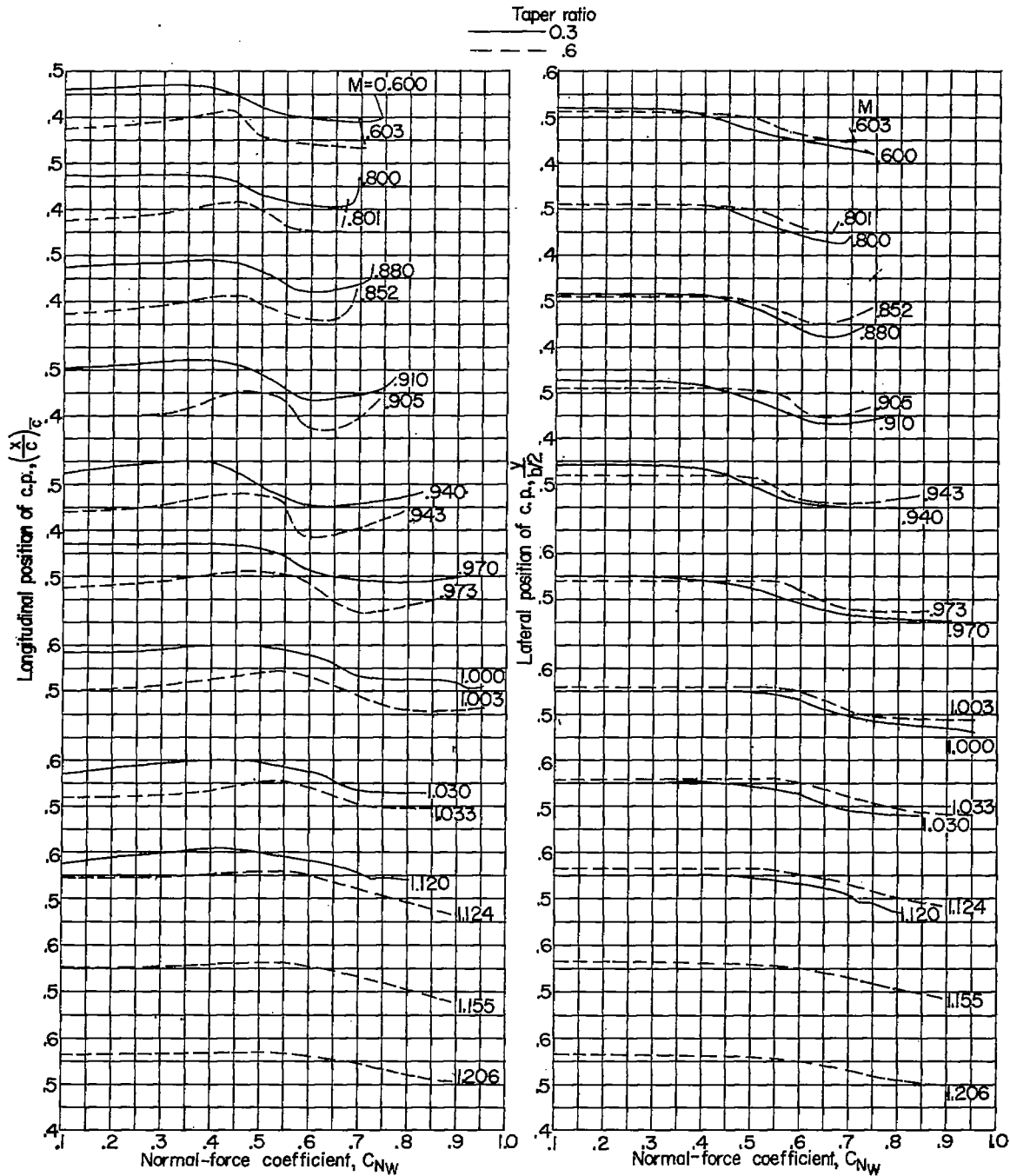
(b) Pitching-moment coefficient.

Figure 10.- Continued.



(c) Bending-moment coefficient. Plain and flagged-right symbols denote data for right and left wings, respectively.

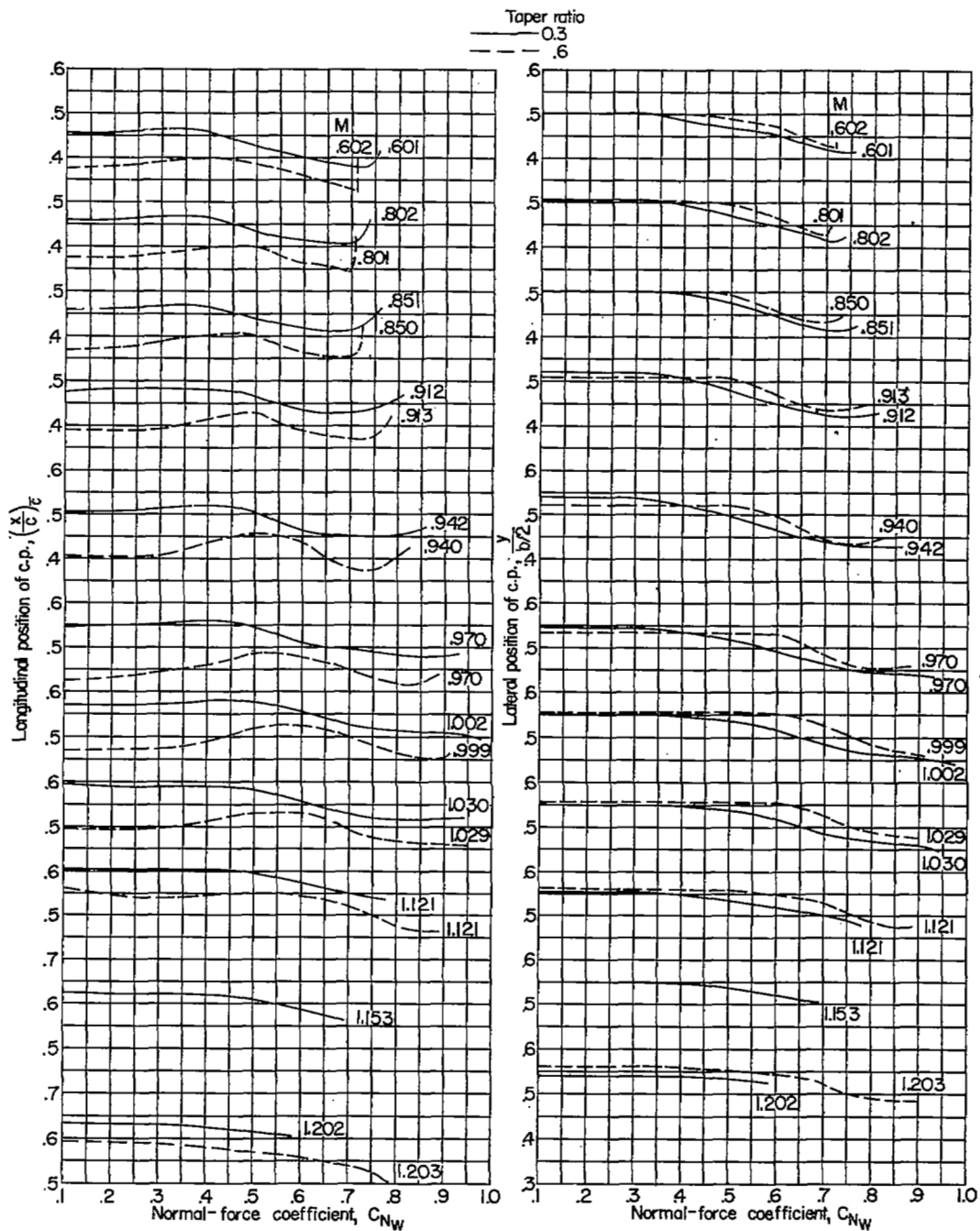
Figure 10.- Concluded.



(a) Variation with wing normal-force coefficient.

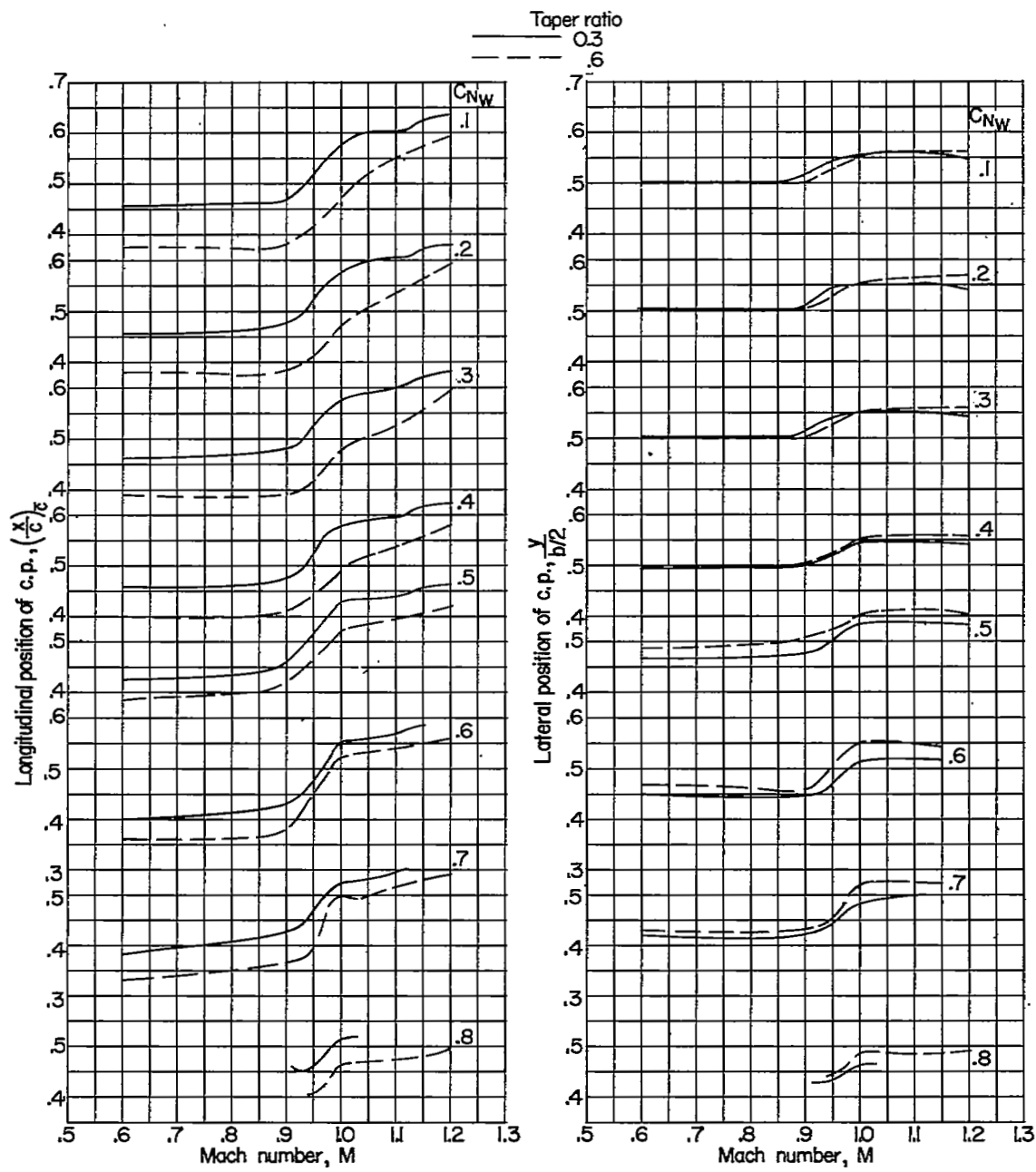
Figure 11.- Effect of taper ratio on variation of longitudinal and lateral location of center of pressure. Basic body.





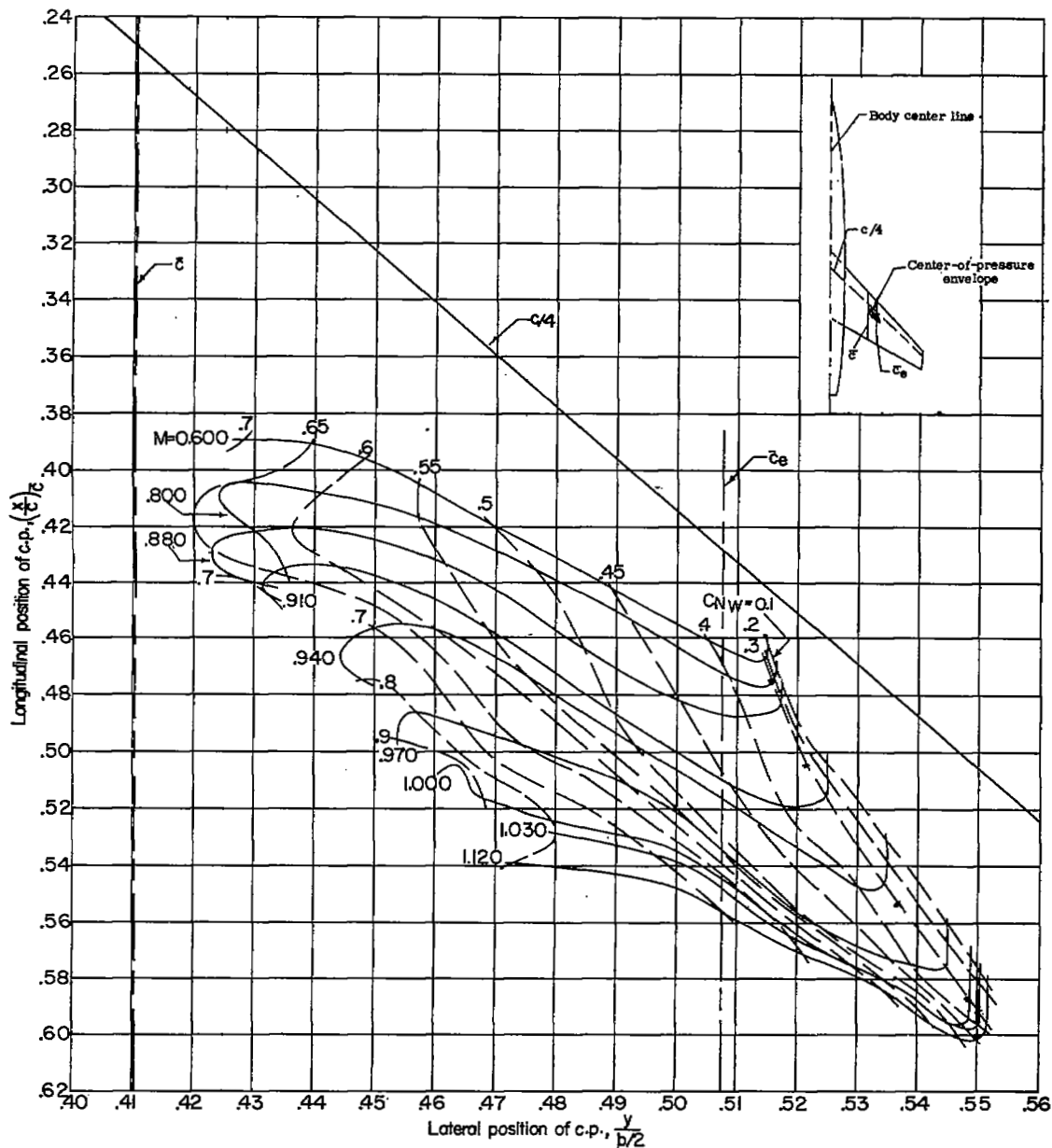
(a) Variation with wing normal-force coefficient.

Figure 12.- Effect of taper ratio on variation of longitudinal and lateral location of center of pressure. Indented body.



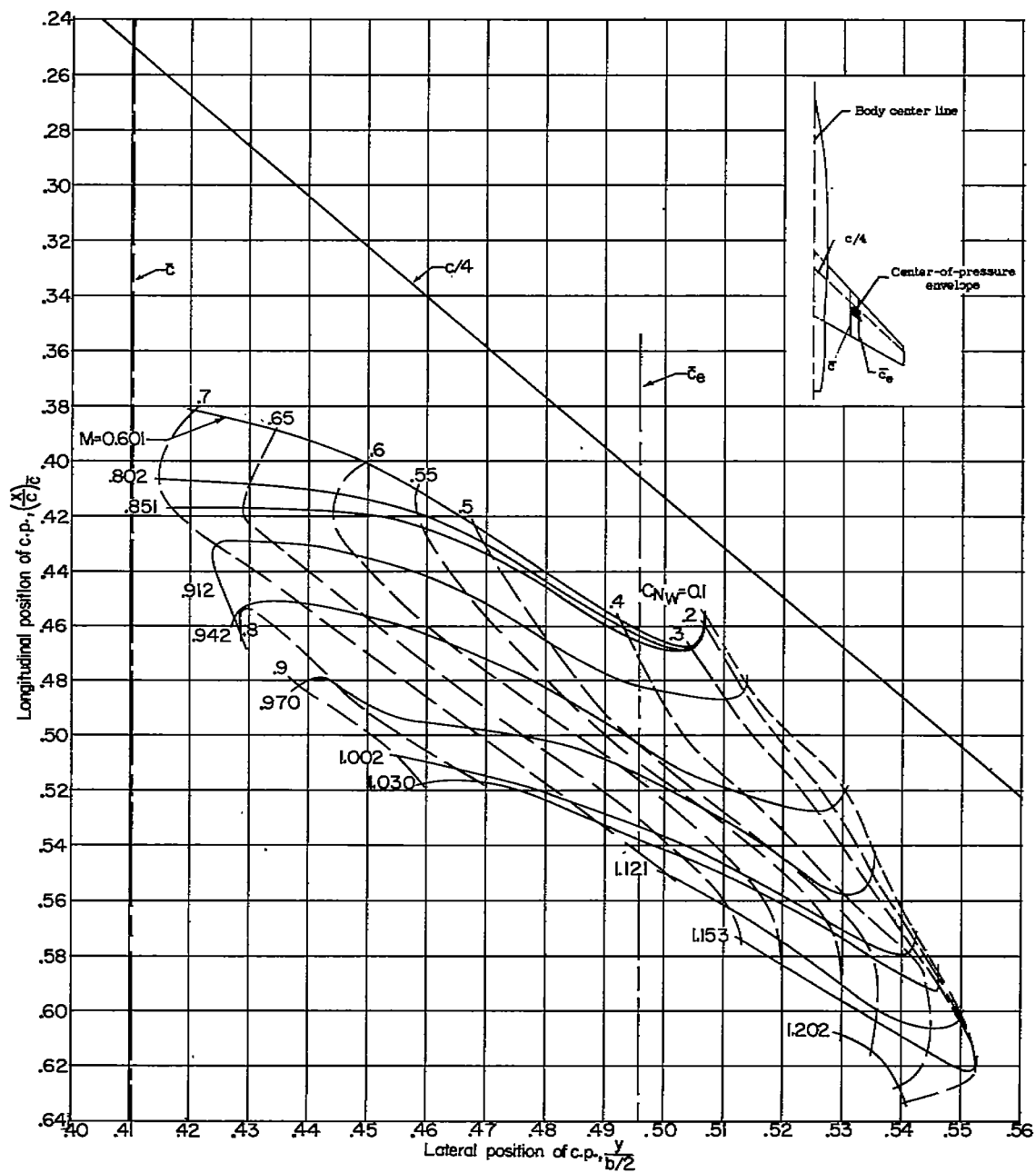
(b) Variation with Mach number.

Figure 12.- Concluded.



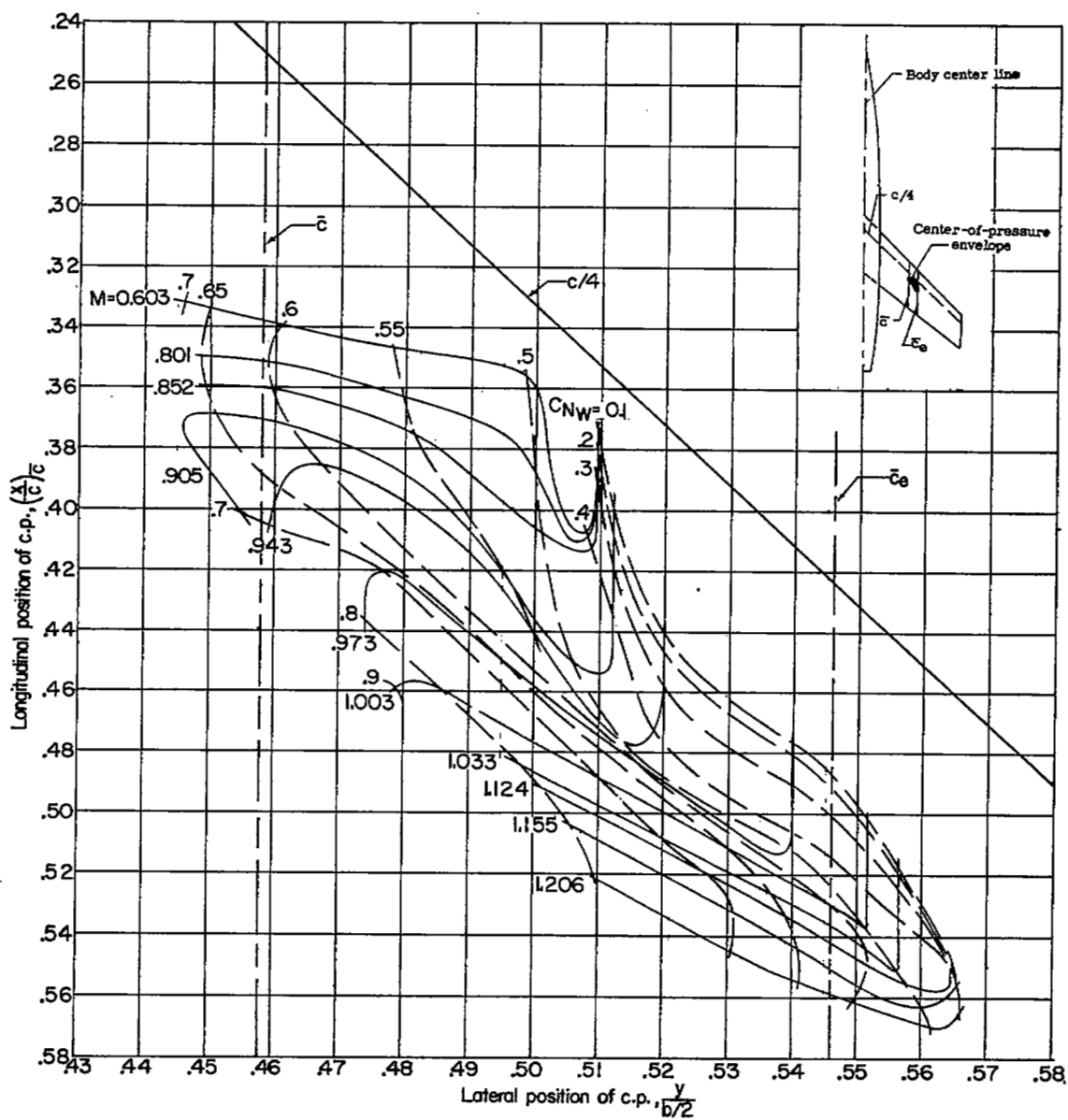
(a) Basic body.

Figure 13.- Variation with Mach number and wing normal-force coefficient of the longitudinal and lateral location of the center of pressure for the 0.3-taper-ratio wing.



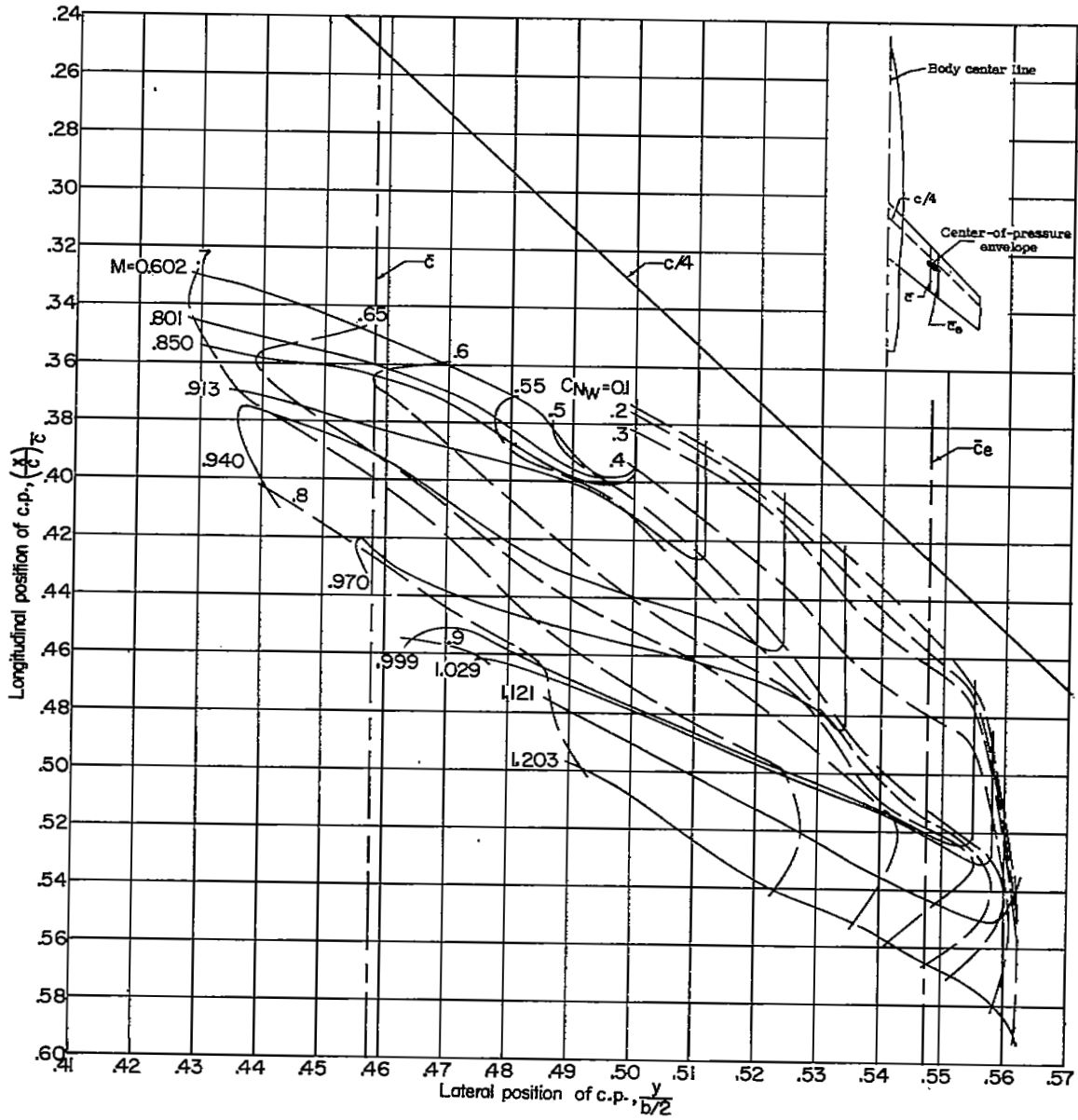
(b) Indented body.

Figure 13.- Concluded.



(a) Basic body.

Figure 14.- Variation with Mach number and wing normal-force coefficient of the longitudinal and lateral location of the center of pressure for the 0.6-taper-ratio wing.



(b) Indented body.

Figure 14.- Concluded.

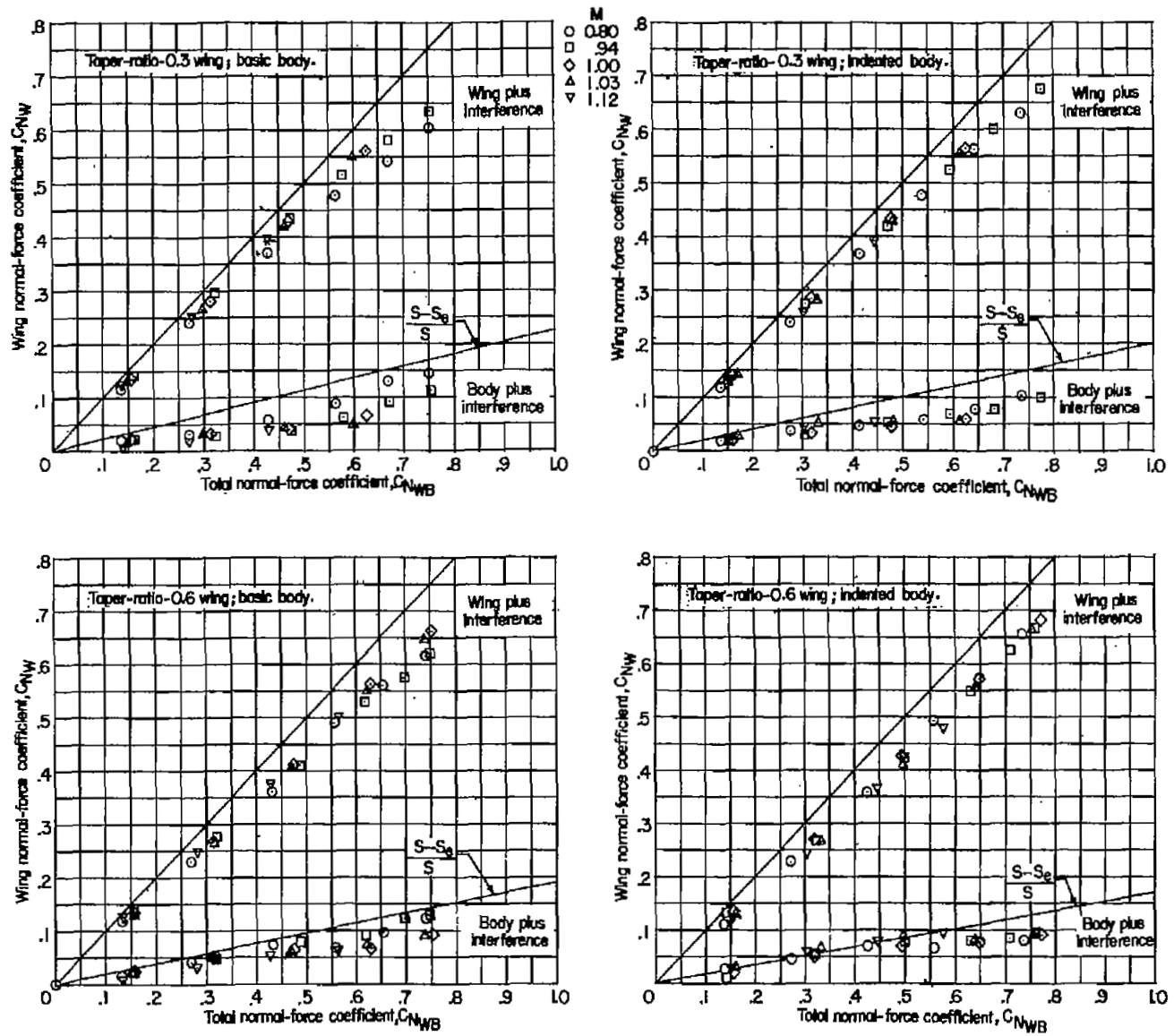
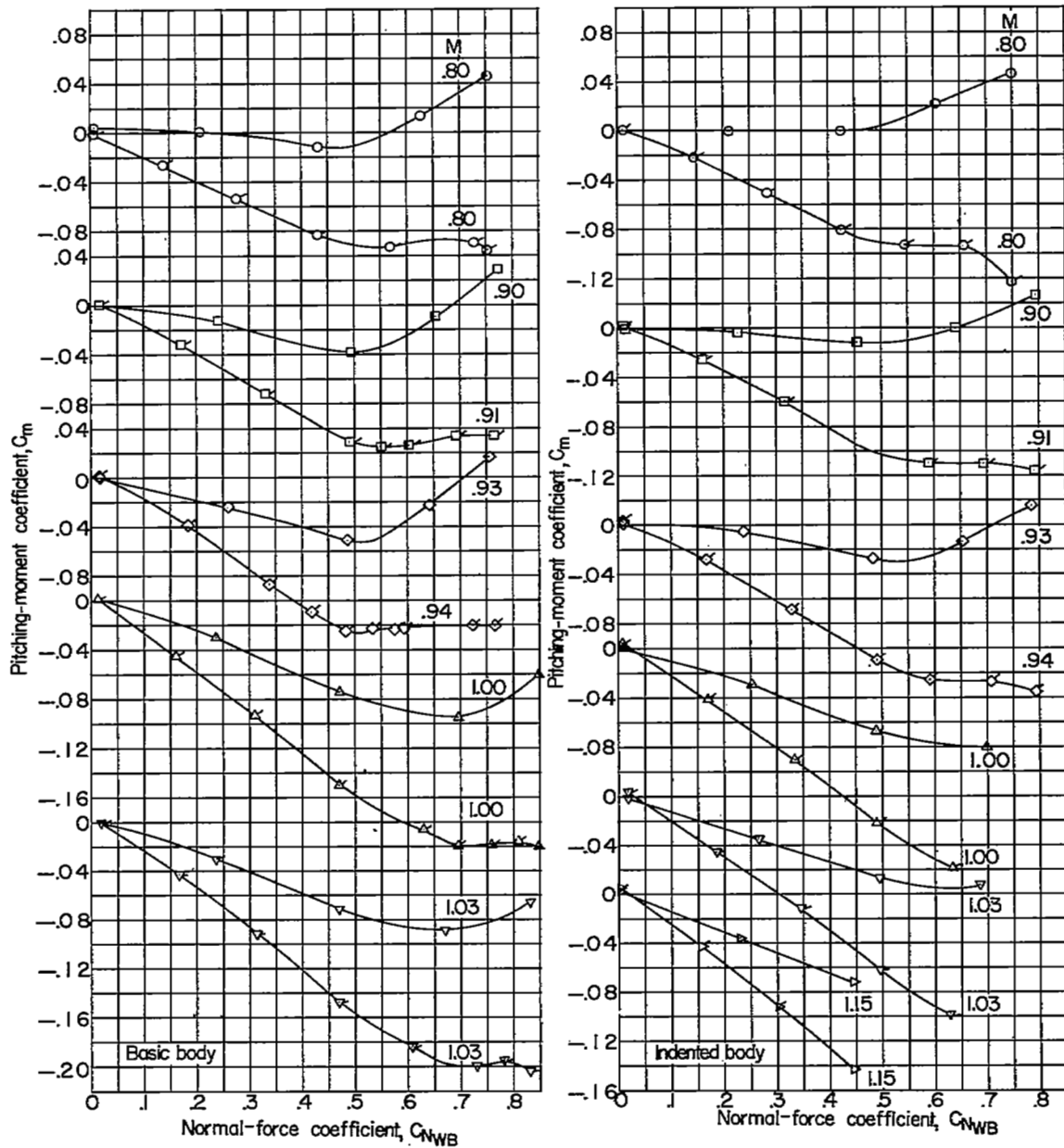
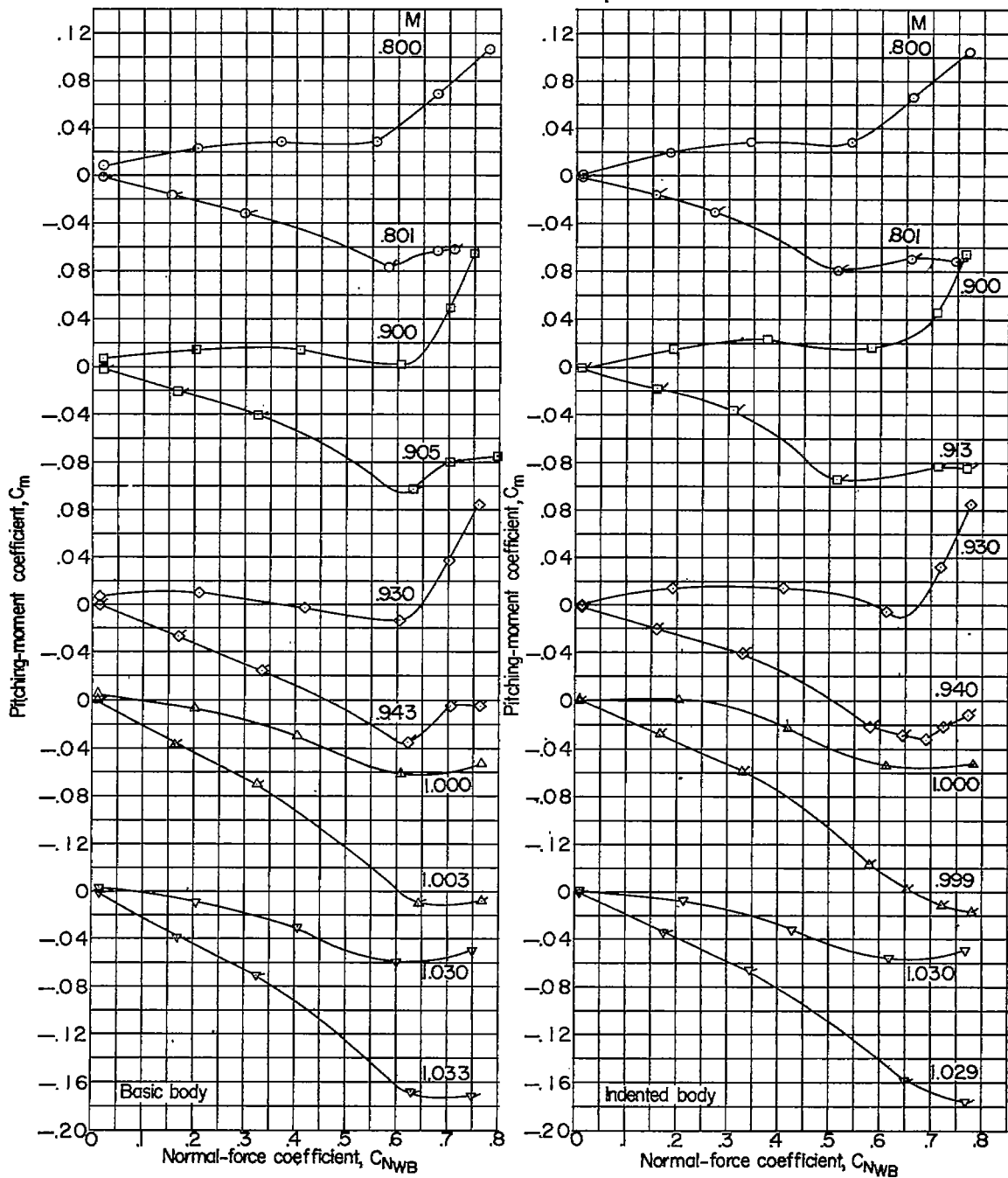


Figure 15.- Division of normal-force load between the wing and body.



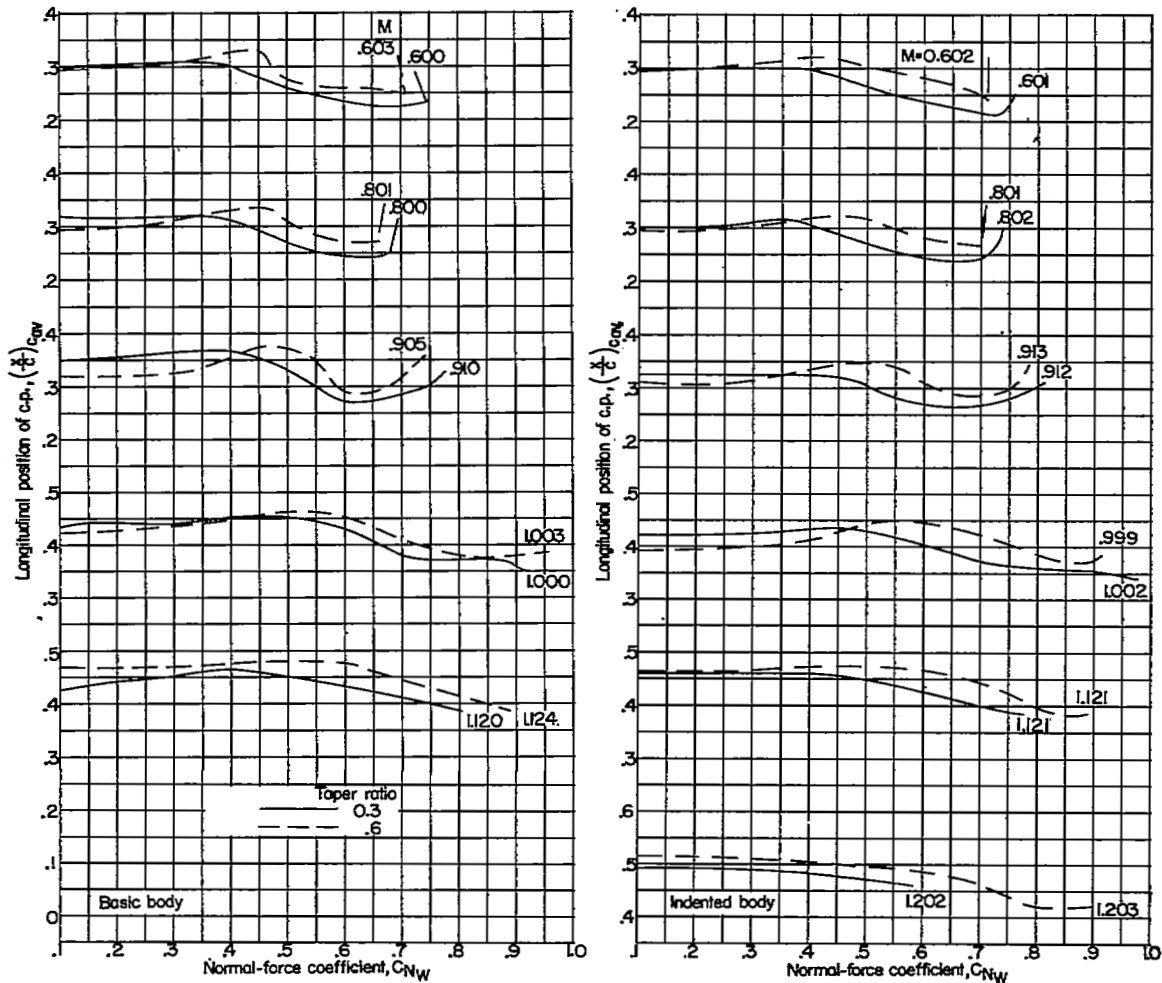
(a) Taper ratio, 0.3.

Figure 16.- Division of pitching-moment load. Plain symbols denote wing-body configuration data; flagged symbols denote wing-plus-interference data.



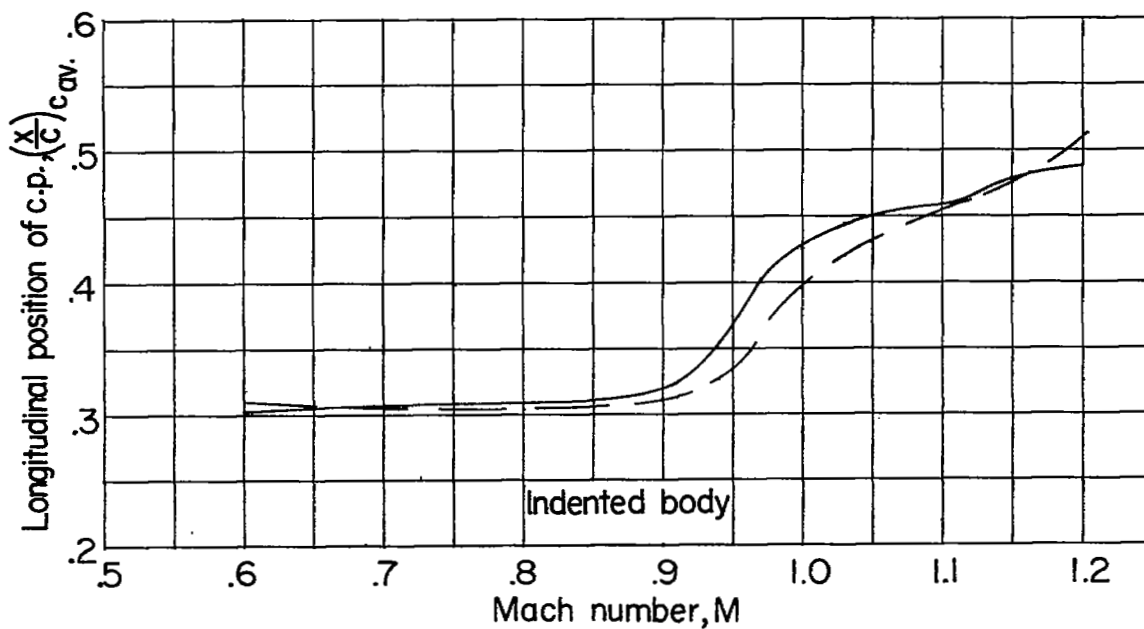
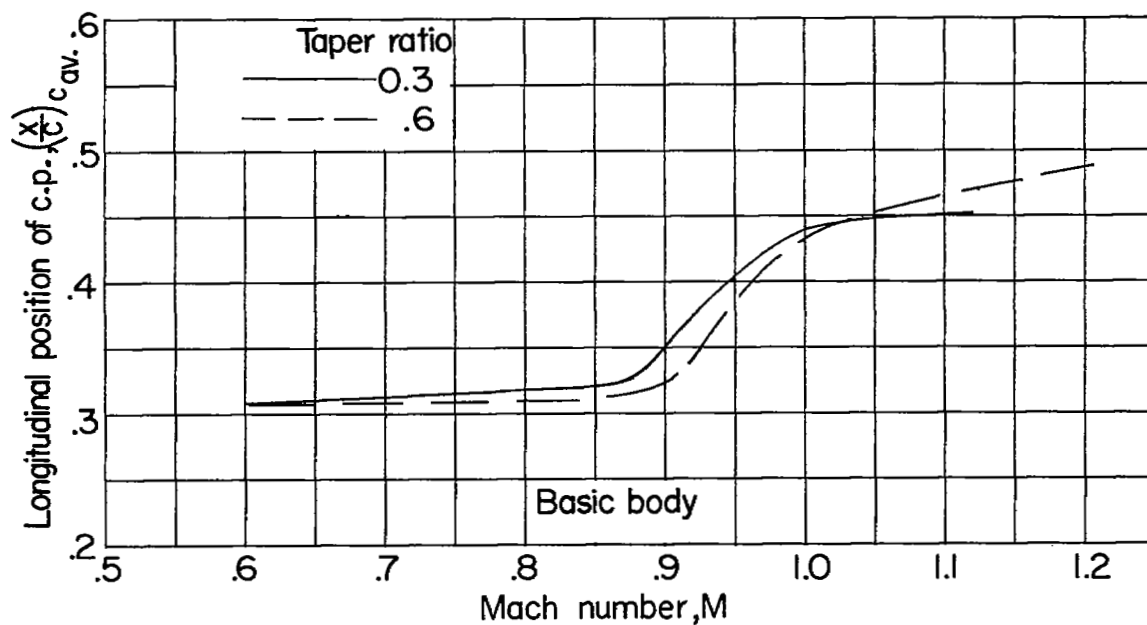
(b) Taper ratio, 0.6.

Figure 16.- Concluded.



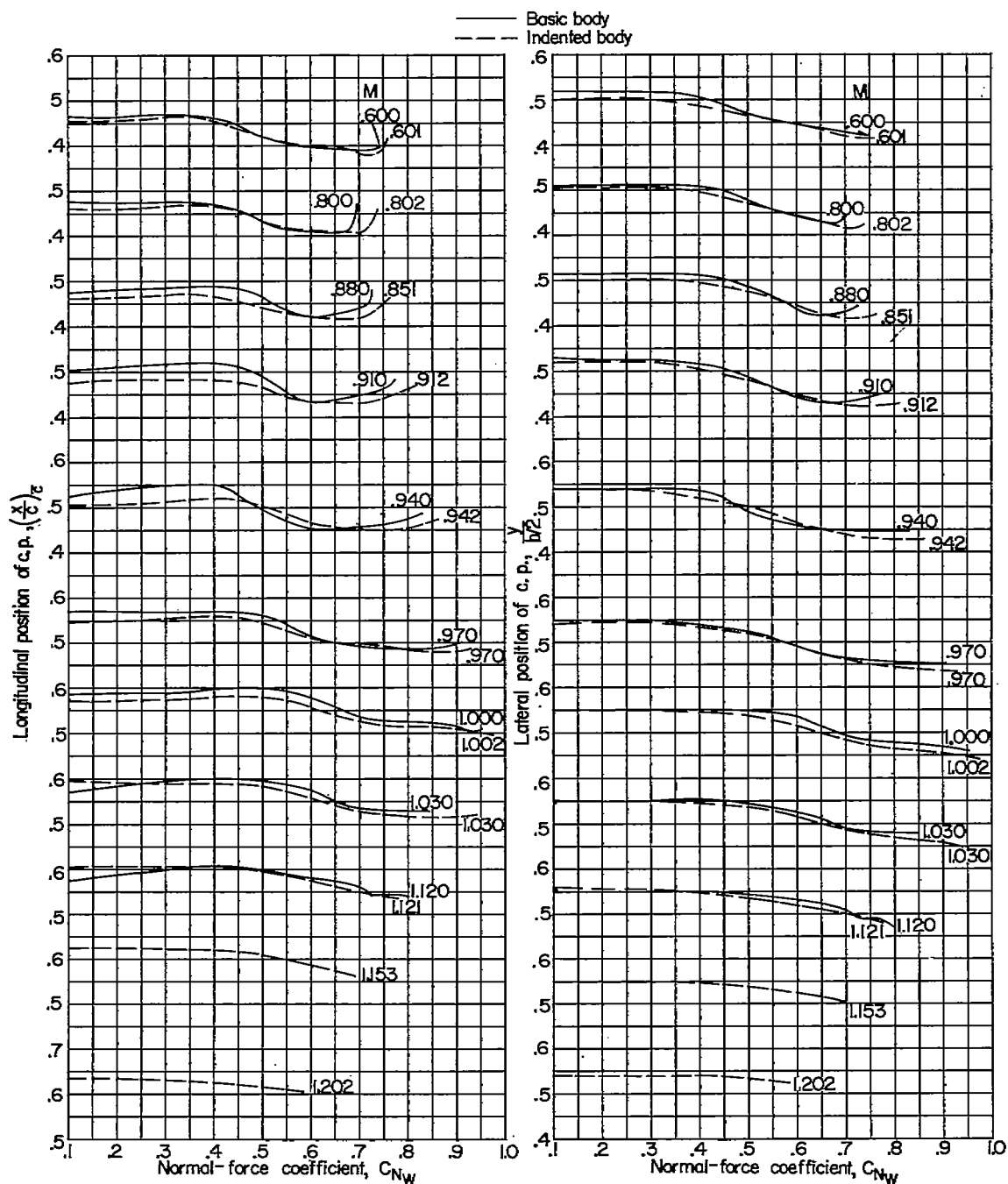
(a) Variation with wing normal-force coefficient.

Figure 17.- Effect of taper ratio on the variation of longitudinal location of center of pressure using the average chord as a reference.



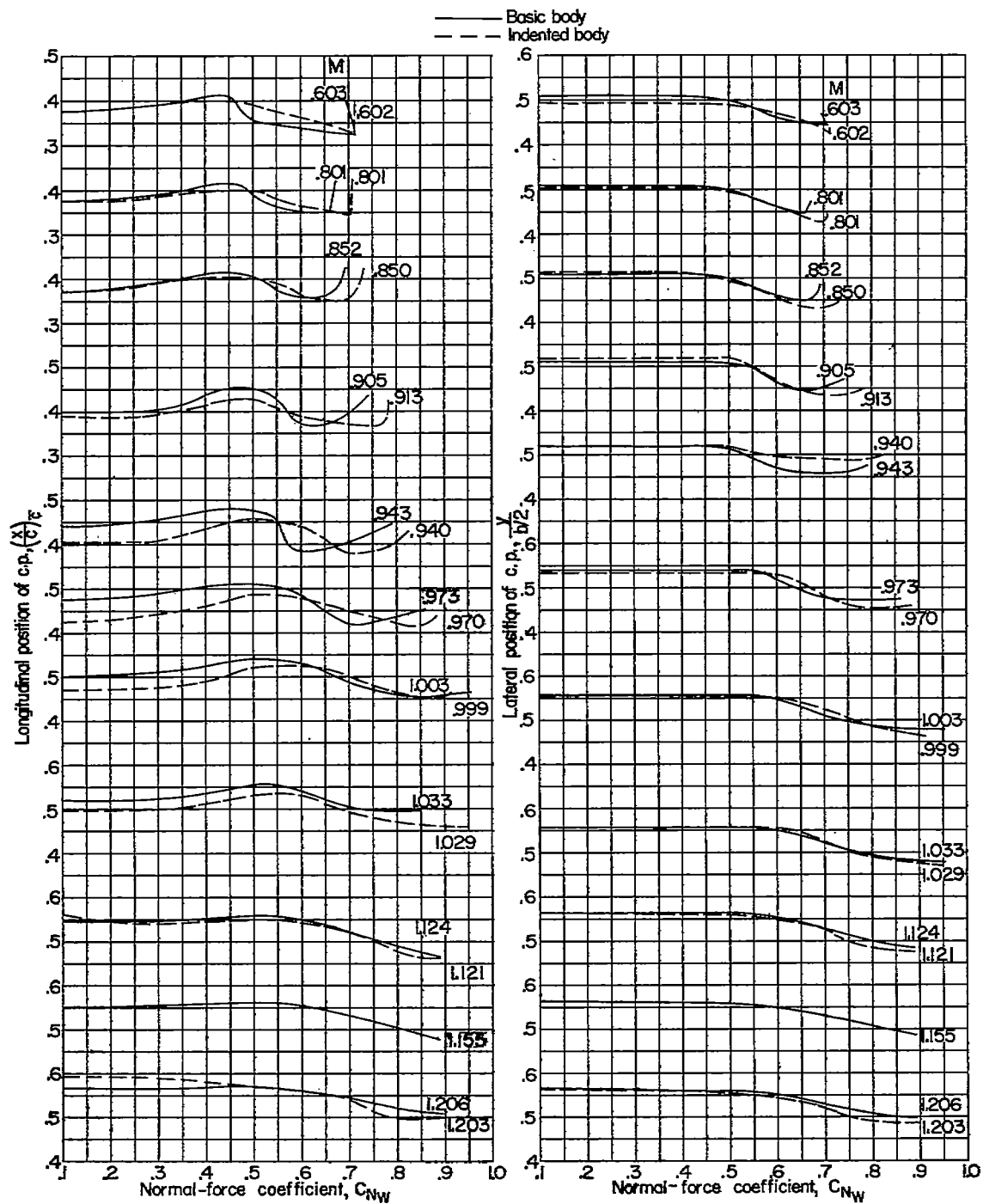
(b) Variation with Mach number.  $C_{N_W} = 0.3$ .

Figure 17.- Concluded.



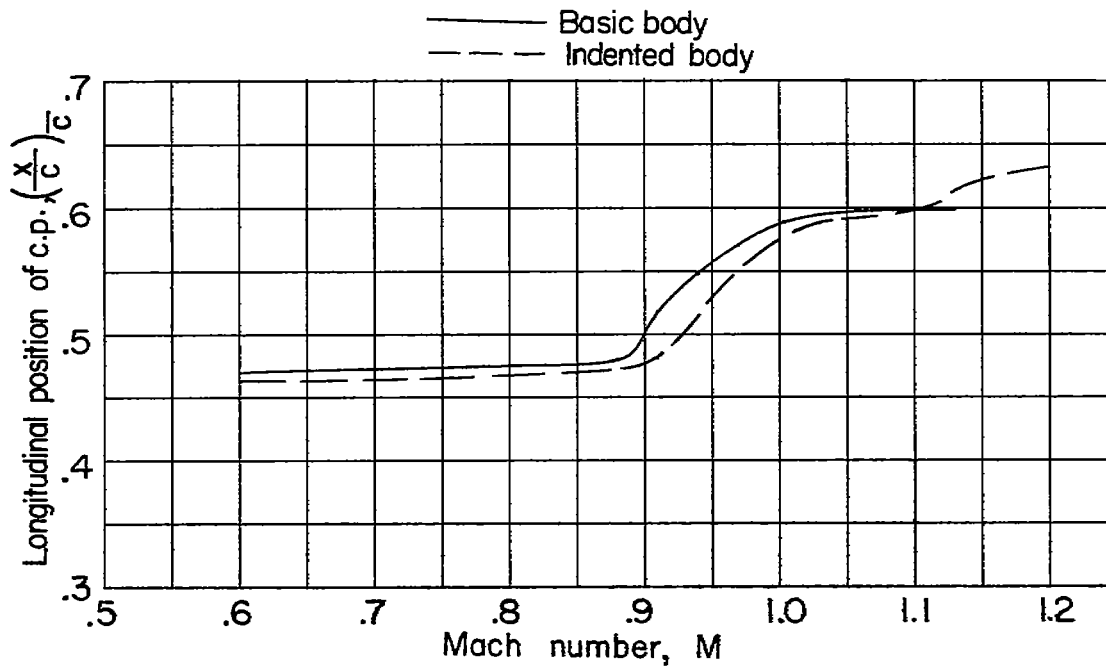
(a) 0.3-taper-ratio wing.

Figure 18.- Effect of body indentation on the variation of longitudinal and lateral location of the center of pressure with wing normal-force coefficient.

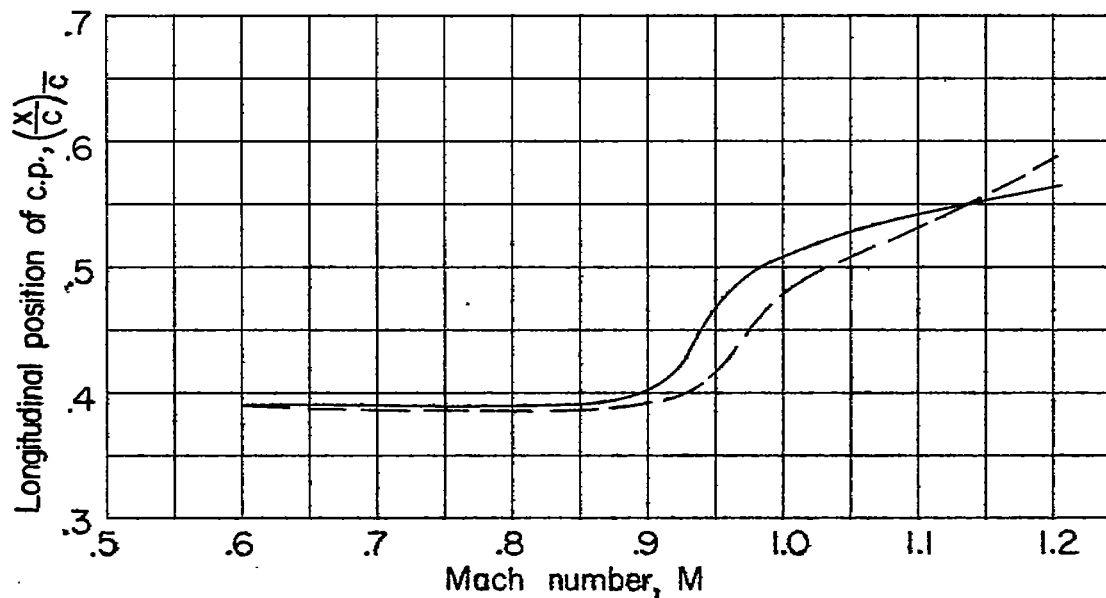


(b) 0.6-taper-ratio wing.

Figure 18.- Concluded.



(a) 0.3-taper-ratio wing.



(b) 0.6-taper-ratio wing.

Figure 19.- Effect of body indentation on the variation of longitudinal position of the center of pressure with Mach number.  $C_{N_W} = 0.3$ .

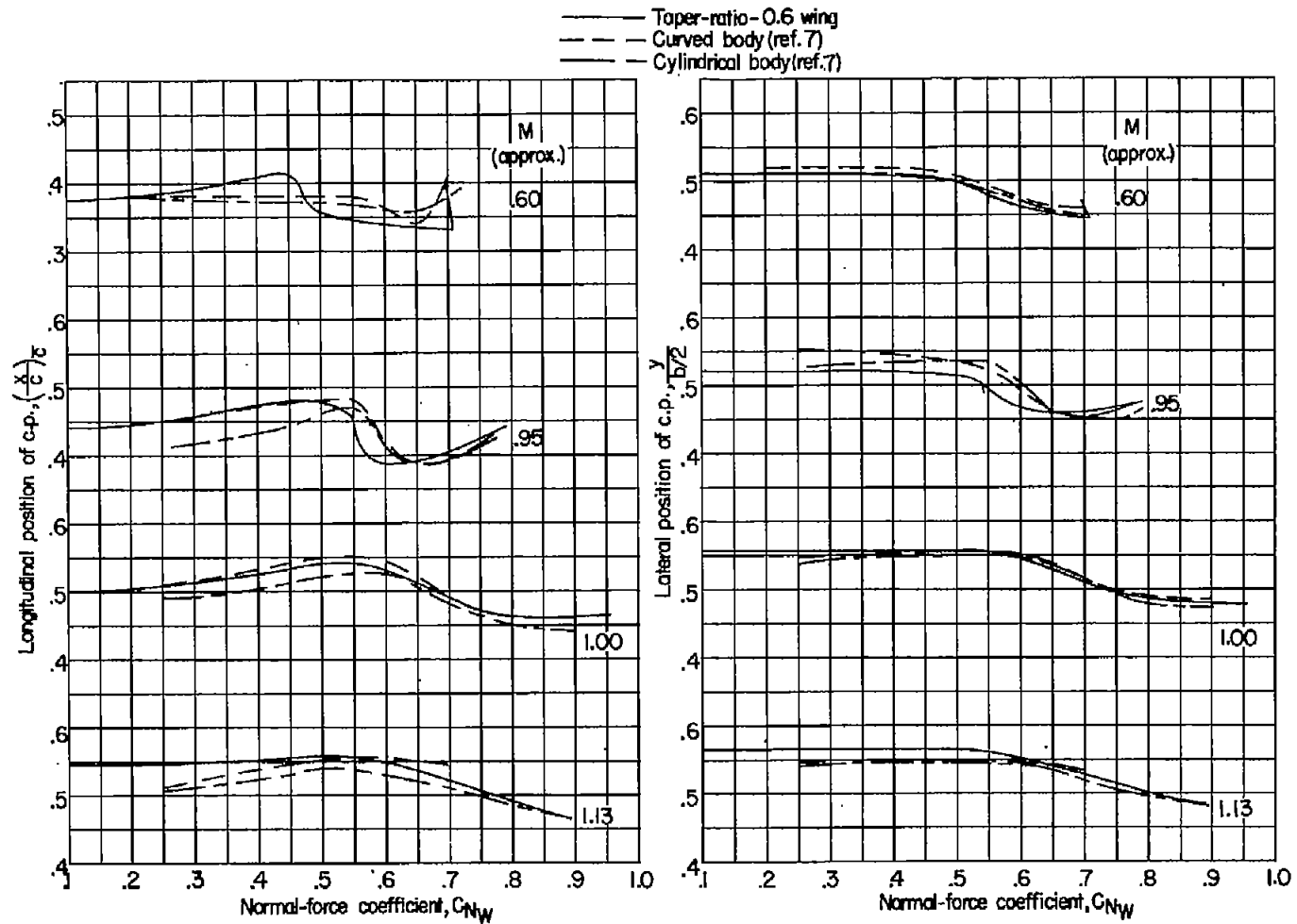


Figure 20.- Comparison of variation of longitudinal and lateral location of the center of pressure with wing normal-force coefficient for the 0.6-taper-ratio wing in the presence of the basic body and for a similar model with two different body configurations of reference 7.

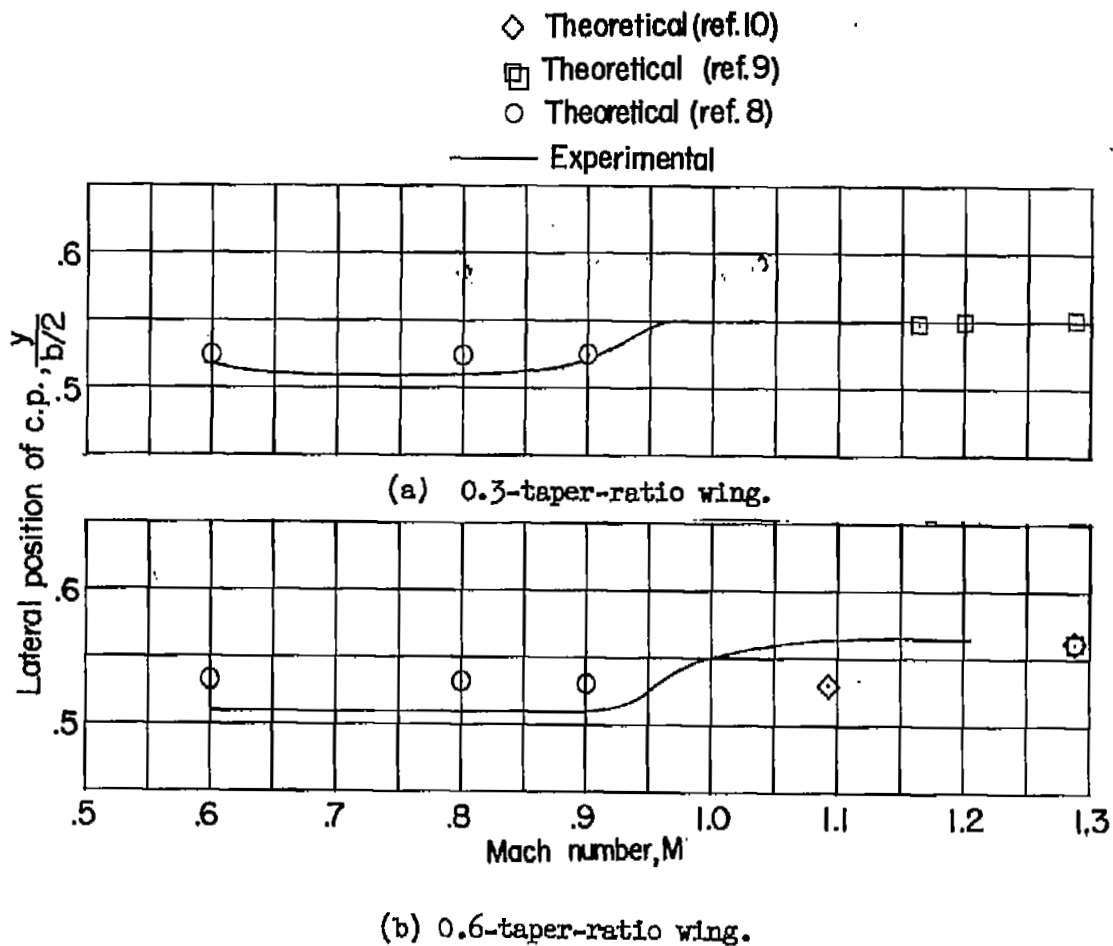


Figure 21.- Comparison of measured values from the basic body configurations and calculated theoretical values of the lateral position of the center of pressure.  $C_{N_w} = 0.3$ .

**CONFIDENTIAL**

NASA Technical Library



3 1176 01437 1976

**CONFIDENTIAL**